ANL/NE-14/9

Update on Developments for the SFR System Analysis Module

Nuclear Engineering Division

About Argonne National Laboratory
Argonne is a U.S. Department of Energy laboratory managed by UChicago Argonne, LLC under contract DE-AC02-06CH11357. The Laboratory's main facility is outside Chicago, at 9700 South Cass Avenue, Argonne, Illinois 60439. For information about Argonne and its pioneering science and technology programs, see www.anl.gov.

DOCUMENT AVAILABILITY

Online Access: U.S. Department of Energy (DOE) reports produced after 1991 and a growing number of pre-1991 documents are available free via DOE's SciTech Connect (http://www.osti.gov/scitech/)

Reports not in digital format may be purchased by the public from the National Technical Information Service (NTIS):
U.S. Department of Commerce
National Technical Information Service
5301 Shawnee
Rd Alexandra,
VA 22312
www.ntis.gov
Phone: (800) 553-NTIS (6847) or (703) 605-6000
Fax: (703) 605-6900
Email: **orders@ntis.gov**

Reports not in digital format are available to DOE and DOE contractors from the Office of Scientific and Technical Information (OSTI):
U.S. Department of Energy
Office of Scientific and Technical Information
P.O. Box 62
Oak Ridge, TN 37831-0062
www.osti.gov
Phone: (865) 576-8401
Fax: (865) 576-5728

Disclaimer
This report was prepared as an account of work sponsored by an agency of the United States Government. Neither the United States Government nor any agency thereof, nor UChicago Argonne, LLC, nor any of their employees or officers, makes any warranty, express or implied, or assumes any legal liability or responsibility for the accuracy, completeness, or usefulness of any information, apparatus, product, or process disclosed, or represents that its use would not infringe privately owned rights. Reference herein to any specific commercial product, process, or service by trade name, trademark, manufacturer, or otherwise, does not necessarily constitute or imply its endorsement, recommendation, or favoring by the United States Government or any agency thereof. The views and opinions of document authors expressed herein do not necessarily state or reflect those of the United States Government or any agency thereof, Argonne National Laboratory, or UChicago Argonne, LLC.

ANL/NE-14/9

Update on Developments for the SFR System Analysis Module

prepared by
R. Hu and T. H. Fanning
Nuclear Engineering Division
Argonne National Laboratory

September 2014

EXECUTIVE SUMMARY

Under the Reactor Product Line (RPL) of DOE/NE's Nuclear Energy Advanced Modeling and Simulation (NEAMS) program, an SFR System Analysis Module is being developed at Argonne National Laboratory for whole-plant safety analysis. This tool will simulate tightly coupled physical phenomena – including nuclear fission, heat transfer, fluid dynamics, and thermal-mechanical response – in SFR structures, systems, and components. It is based on the MOOSE (Multi-physics Object-Oriented Simulation Environment) framework, which relies upon open-source libraries such as libMesh and PETSc for mesh generation, finite element analysis, and numerical solutions. The SFR System Analysis Module is aimed to model and simulate SFR systems with higher fidelity and with well-defined and validated prediction capabilities. It will provide fast-running, modest-fidelity, whole-plant transient analyses capability, which is essential for fast turnaround design scoping and engineering analyses.

Most effort in FY13 was focused on the development of component models using the conservative variable based (or density-based) formulations in collaboration with the RELAP-7 effort for the purpose of developing the SFR primary system modeling capability in a shorter time. In FY14, the primitive variable based (or pressure-based) flow model was demonstrated to have superior convergence performance compared to the conservative variable based flow model for incompressible flows. Therefore, the focus was shifted toward developing integrated-physics components using the primitive variable based flow model in FY14.

In FY14, the 1-D FEM flow model using a primitive variable based formulation with numerical stabilization schemes has been improved for use in the incompressible sodium flows. It is confirmed that the developed FEM flow model can be strictly verified, and that it performs very well for a wide range of flow problems, including density wave propagation where numerical instability and numerical diffusion can be eliminated by its second-order numerical accuracy in both space and time; steep gradient problems where steep gradient can be handled and only slightly smoothed; discharging between tanks where flow reversal and a wide range of flow conditions (convection dominant or not) are modeled; and the flow and heat transfer in a heat exchanger where the conjugate heat transfer problem is accurately solved in a fully-coupled fashion and the second-order accuracy is verified.

A set of general and SFR-specific physics models and component has also been developed in FY14 based on the primitive variable based flow model. The simulation of the ABTR PLOF transient and the EBR-II SHRT-17 test has successfully demonstrated the SFR system simulation capabilities using the new set of Components, while also demonstrating its superior performance compared to the original density-based flow solver. In the ABTR PLOF simulations, almost identical flow rates were predicted for both the pump coastdown and the natural circulation phases between the pressure-based and the density-based flow models. However, the comuting time for the 1000 second transient is significantly reduced from ~2 hours to ~8 minutes with the pressure-based flow model. The transient response of the core flow in the simulation is also similar to that from the EBR-II SHRT-17 test, although the magnitudes are slightly different. Further investigations will be needed to resolve or better understand the causes of the differences between the simulation and experiment results.

Although it is a relatively new effort, the SFR System Analysis Module development and the recent progress are very encouraging. It can be confirmed that the major physics phenomena in SFR primary coolant loop during the protected-loss-of-flow transients can be well captured by the SFR System Analysis Module simulations, and that the new flow model can significantly improve the code convergence speed for the incompressible but thermally expandable flow systems. The next stage of the development will be continued on component designs and physics integration for SFR analysis, demonstration of code capabilities through simulations of SFR design base accidents or design extension conditions, and code verification and validation. Additionally, the integration with other high-fidelity advanced simulation tools developed under the NEAMS Program, such as Nek-5000, will be investigated to pursue a multi-scale multi-physics simulation using the integrated NEAMS RPL tools.

TABLE OF CONTENTS

Executive Summary i

Table of Contents iii

List of Figures iv

List of Tables iv

1 Introduction 1

2 Overview of SFR System Analysis Module Development 3

2.1 Development Approach 3
2.2 Overview of Current Capabilities 4
2.3 Multi-Scale Code Coupling 7
2.4 Advantages over Current System Codes 8

3 An advanced One-D FEM Flow Model and Verification 10

3.1 Governing Equations 10
3.2 SUPG/PSPG Stabilization and the Solution Scheme 12
3.3 Verification Tests 15
3.3.1 Density Wave Oscillations 15
3.3.2 Steep Gradient Problems 17
3.3.3 Tank Discharge Problem 20
3.3.4 Conjugate Heat Transfer Problems 20

4 Demonstration Simulation of ABTR 23

4.1 Model Description 23
4.2 Accident Sequences 24
4.3 Simulation Results 25

5 Simulation of EBR-II SHRT-17 Test 29

5.1 Model Description 29
5.2 Simulation Results 30

6 Summary 38

References 39

LIST OF FIGURES

Figure 1: The Structure of the SFR System Analysis Module 4
Figure 2: Temperature Distribution in a Coupled System and CFD Transient Simulation 8
Figure 3: An example of non-physical (numerical) pressure oscillation 12
Figure 4: Transient responses of the pipe under inlet temperature oscillation, BDF2 16
Figure 5: Damped temperature wave under inlet temperature oscillation, backward Euler 17
Figure 6: Smoothing of steep gradient during a temperature step change transient 18
Figure 7: Smoothing of steep gradient during a temperature pulse transient 19
Figure 8: Flow velocity response during a pressure step change transient 19
Figure 9: Transient response of the tank discharge test 20
Figure 10: Temperature distribution of a counter-current heat exchanger 21
Figure 11: Temperature difference distribution of a counter-current heat exchanger 22
Figure 12: Spatial convergence study of a counter-current heat exchanger 22
Figure 13: Schematics of the test ABTR model 24
Figure 14: Normalized power and pump head history during PLOF 25
Figure 15: Normalized power and core flow during the PLOF transient 27
Figure 16: Core channel flow velocities during the PLOF transient 27
Figure 17: Heat removal rate from IHX during the PLOF transient 28
Figure 18: Pool temperatures during the PLOF transient 28
Figure 19: EBR-II Plant Model for SHRT-17 [17] 30
Figure 20: Temperatures distribution of EBR-II at steady-state 31
Figure 21: Temperatures response during steady state initialization 31
Figure 22: Normalized power and pump head history during SHRT-17 test 32
Figure 23: Comparison of core flow rate during the SHRT-17 test 34
Figure 24: Comparison of core outlet temperatures during the SHRT-17 test 34
Figure 25: Comparison of IHX Inlet temperature during the transient 35
Figure 26: IHX inlet and outlet temperature responses, the effect of Z-Pipe heat loss 35
Figure 27: Core flow rate responses during SHRT-17 test, the effect of Z-Pipe heat loss 36
Figure 28: IHX heat removal rate response during the SHRT-17 test 36
Figure 29: Inner and outer core flow responses during the SHRT-17 test 37

LIST OF TABLES

Table 1. Major SFR System Analysis Module Components, based on the primitive variable formulation 5
Table 2. Key Features Comparison between Traditional System Tools and SFR System Analysis Module 9

1 Introduction

System thermal-hydraulics is one of the major disciplines essential for the design, licensing, and operation of nuclear systems. Many system analysis codes, such as RELAP5 [1], CATHARE [2] and SAS4A/SASSYS-1 [3], have been developed since the early 1970s and successfully applied for the design, license, and operational analysis of the nuclear power plants. Although these codes have achieved a certain level maturity, they have not taken full advantage of the rapid expansion in computing power and advances in numerical methods over the past two decades.

With advances in numerical techniques and software engineering, such as the availability of non-linear solvers and object-oriented application frameworks, modernization of existing systems codes or the development of new system codes becomes more compelling. For example, RELAP-7 [4], an advanced safety analysis tool for light-water reactors, is being developed on the MOOSE [5] framework to interface with libMesh [6] and PETSc [7] to provide the underlying geometry (mesh I/O) and numerical capabilities (finite element library and solvers). RELAP-7 itself defines objects on this interface that represent typical components and systems in a light water reactor (LWR). Similar developments are being pursued for components and systems that represent typical features of advanced reactor concepts such as SFRs (sodium fast reactors), LFRs (lead-cooled fast reactors), and FHRs (fluoride-salt-cooled high temperature reactors). These advanced reactor concepts are distinguished from light-water reactors in their use of single-phase, low-pressure, very low Prandtl number coolants that undergo higher temperature changes. This simple yet fundamental change has significant impacts on core and plant design, the types of materials used, component design and operation, fuel behavior, and the significance of the fundamental physics in play during transient plant simulations. These advanced system simulation development efforts are referred to as the SFR System Analysis Module (SAM) to highlight its current focus and to distinguish the modeling needs of advanced reactor concepts from light-water reactors.

The SFR System Analysis Module is being developed for sodium fast reactor simulations under U.S. DOE-NE's Nuclear Energy Advanced Modeling and Simulation (NEAMS) program. Its goal is to solve the tightly-coupled physical phenomena including fission reaction, heat transfer, fluid dynamics, and thermal-mechanical response in the SFR structures, systems and components in a fully-coupled fashion but with reduced-order modeling approaches to facilitate rapid turn-around for design and safety optimization studies. Additionally, the integration with other high-fidelity advanced simulation tools developed under the NEAMS Reactor Product Line (RPL) is being pursued for a multi-scale multi-physics simulation using the integrated NEAMS RPL toolkit. For example, the SFR System Analysis Module would provide system responses and transient boundary conditions for detailed Nek5000/Proteus/Diablo simulations of the reactor core in the safety analysis of postulated reactor transients.

This report provides an update of the SFR System Analysis Module developments in FY14. The code development approach and current capabilities are summarized in Section 2. Section 3 describes the updates of the underlying one-dimensional systems-level thermal-hydraulics simulation capabilities in which the primitive variable based (or pressure-based) fluid model and its verification are discussed. A new set of Components for reactor system

simulation has also been developed based on the primitive variable based fluid model. Section 4 discusses the demonstration simulation of protected loss of flow (PLOF) transient in the Advance Burner Test Reactor (ABTR) [8]. The IAEA coordinated benchmark exercise of EBR-II SHRT-17 test is discussed in Section 5. Finally, Section 6 provides a summary of the FY14 effort and the direction needed for future code development work.

2 Overview of SFR System Analysis Module Development

2.1 Development Approach

The goal of the SFR System Analysis Module is to provide system-level modeling and simulation tools with much higher fidelity and with well-defined and validated prediction capabilities for SFR systems. It will provide fast-running, modest-fidelity, whole-plant transient analyses capability, which is essential for fast turnaround design scoping and engineering analyses and could lead to improvements in the design of new reactors, the reduction of uncertainties in safety analysis, and reductions in capital costs. To fulfill its objectives, the SFR System Analysis Module

- utilizes an object-oriented application framework (MOOSE), the underlying meshing and finite-element library, and non-linear solvers (LibMesh and PETSc) to leverage the available advanced software environments and numerical methods.
- incorporates advances in the physical and empirical models for SFR system analysis developed over the past several decades.
- provides multi-scale multi-physics modeling capabilities by integrating with other higher-fidelity advanced simulation tools.

The SFR System Analysis Module was also a coordinated development effort with RELAP-7. It can leverage the common features between LWRs and SFRs, and the existing RELAP-7 physics models and component library can be available for use in the SFR System Analysis Module as dependent libraries if needed (see Figure 1). For example, the two-phase flow model and the component library in RELAP-7 could be used for the steam generator and balance-of-plant simulation in conjunction with the SFR System Analysis Module for reactor core and primary loop simulation. This tool also provides

- 1-D FEM flow models using a primitive variable based formulation with numerical stabilization schemes for use in incompressible sodium flows.
- multi-scale, single-phase flow coupling capabilities between the SFR System Analysis Module and any CFD code to simulate multidimensional phenomena, such as thermal stratification.
- integrated component models for SFR system, structure, and components based on the primitive variable based flow model.
- verification and demonstration problems for both stand-alone system simulation capabilities and coupled multi-scale or multi-physics simulation capabilities.

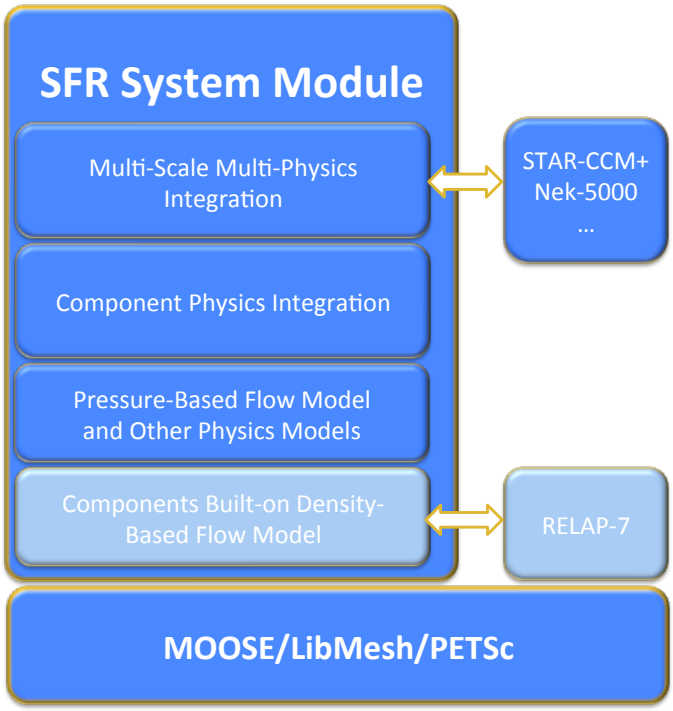

Figure 1: The Structure of the SFR System Analysis Module

2.2 Overview of Current Capabilities

To develop a system analysis code, numerical methods, mesh management, equations of state, fluid properties, solid material properties, neutronics properties, pressure loss and heat transfer closure laws, and good user input/output interfaces are all indispensible. The SFR System Analysis Module leverages the MOOSE framework and its dependent libraries to provide JFNK solver schemes, mesh management, and I/O interfaces while providing new physics and component models to model the SFR systems.

A numerically stable scheme for continuous finite element analysis of single-phase flow has been developed for non-LWR advanced reactor applications. It uses primitive variable (or pressure) based formulation, while the RELAP-7 code uses the conservative variable (or density) based formulations. Although the conservative variable based formulation has many advantages in the applications of compressible flow, such as the capability to capture the shock waves, the primitive variable based FEM formulation is more suitable for incompressible or nearly incompressible flows, such as the fluid flow in the SFRs, LFRs, or FHRs. To prevent potential numerical instability issues, the stabilization techniques of incompressible flows were extensively reviewed, and the Streamline-Upwind Petrov-Galerkin (SUPG) and the Pressure-Stabilizing Petrov-Galerkin (PSPG) formulations [9] have been chosen and implemented as the stabilization schemes. More details on the flow model and stabilization scheme will be discussed in Section 3.

It should be noted that most effort in FY13 was focused on the development of component models using the conservative variable based formulations in collaboration with the RELAP-7 effort for the purpose of developing the SFR primary system modeling capability in a shorter time. In FY14, the primitive variable based flow model was demonstrated to have superior

convergence performance compared to the conservative variable based flow model for incompressible flows. Therefore, the focus was shifted toward developing integrated-physics components using the primitive variable based flow model in FY14.

The physics modeling and mesh generation of individual reactor components are encapsulated as Component classes. A new set of components has been developed using the primitive variable based FEM formulation, as listed in Table 1, including: (1) 1-D components such as pipe, core channel, and heat exchanger; (2) 0-D components for setting boundary conditions such as time dependent volume, time dependent junction, and time dependent mass flow rate; and (3) 0-D components for connecting 1-D components such as junctions, branches, and pumps.

Table 1. Major SFR System Analysis Module Components, based on the primitive variable formulation

Component name	**Descriptions**	**Dimension**
OneDFluidComponent	Simulates 1-D fluid flow using the primitive variable formulation	1-D
CoupledHeatStructure	The heat structure connecting two liquid components (1-D or 0-D).	2-D or 3-D
Pipe	Simulates the fluid flow in a pipe and the heat conduction in the pipe wall.	1-D fluid, 2-D or 3-D structure
HeatExchanger	Simulates a heat exchanger, including the fluid flow in the primary and secondary sides, convective heat transfer, and heat conduction in the tube wall.	1-D fluid, 2-D or 3-D structure
CoreChannel	Simulates reactor core channels, including 1-D flow channel and the inner heat structure of the fuel rod, and the outer heat structure of the duct wall.	1-D fluid, 2-D or 3-D structure
DuctedCoreChannel	Simulates reactor core channels with an outer heat structure of the duct wall.	1-D fluid, 2-D or 3-D structures
BypassChannel	Models the bypass flow in the gaps between fuel assemblies.	1-D
FuelAssembly	Models reactor fuel assemblies composed of multiple CoreChannels, representing different regions of a fuel assembly (core, gas plenum, reflector, shield, etc.).	1-D fluid, 2-D or 3-D structure
DuctedFuelAssembly	Model reactor fuel assemblies composed of multiple DuctedCoreChannels.	1-D fluid, 2-D or 3-D structure

ReactorCore	Models a pseudo three-dimensional reactor core; It consists of member core channels (with duct walls) and bypass channels.	0-D
Branch	Models a zero-volume flow joint, where multiple 1-D fluid components are connected.	0-D
SingleJunction	Models a zero-volume flow joint, where two 1-D fluid components are connected.	0-D
Pump	Simulates the pump component, in which the pump head is dependent on a pre-defined function.	0-D
VolumeBranch	Considering the volume effects of a flow joint so that it can account for the mass and energy in-balance between the inlets and outlets due to inertia	0-D
CoverGas	A 0-D gas volume that is connected to one or multiple liquid volumes.	0-D
LiquidVolume	The 0-D liquid volume with cover gas, thus the liquid volume can change during the transient.	0-D
TDJ	An inlet boundary in which the flow velocity and temperature are provided by pre-defined functions.	0-D
TDV	A boundary in which the pressure and temperature conditions are provided by pre-defined functions.	0-D
CoupledTDV	A TDV boundary in which the boundary conditions are provided by other codes in coupled code simulation.	0-D

The developed physics models and components provide several major modeling features:

1. One-D pipe networks to represent general fluid systems such as the reactor coolant loops;
2. Flexible integration of fluid and solid components, able to model complex and generic engineering system.
3. A three-dimensional capability to model the radial heat-transfer in the reactor core; The heat generated in the fuel rod of one fuel assembly can be transferred to the coolant in the core channel, the duct wall, the inter-assembly gap, and then the adjacent fuel assemblies. This is particularly important for SFR since the thermal conductivity of the sodium is very high, so that the radial heat conduction through the inter-assembly gap is important for accurate temperature prediction throughout the reactor core. A general liquid flow and solid structure interface model was developed for easier implementation of physics models in the components.
4. SFR (pool-type) specific features such as liquid volume level tracking, cover gas dynamics, heat transfer between 0-D pools, fluid heat conduction, etc. These are

important features for accurate SFR safety analysis. For example, the heat transfer from the hot pool to the cold pool would affect the temperatures and liquid levels of the pools, thus significantly affect the natural circulation flow rate in the primary loop and other behaviors during SFR transients.

2.3 Multi-Scale Code Coupling

In addition to the physics and component module development, a multi-scale integration capability was also added to the SFR System Analysis Module to allow coupled code simulations between the system code and other higher fidelity tools. For practical nuclear engineering applications, multi-scale analysis by adopting the combined use of different scale computational tools, such as system thermal-hydraulics and CFD codes, is vital when three-dimensional effects play an important role in the evolution of a given transient or accident scenario. This capability is also important for the integration between the System Analysis Module and other high-fidelity advanced simulation capabilities developed under the NEAMS RPL.

Careful control of data exchange and time-synchronization is essential for a numerically stable and physically valid coupled code simulation. The general issues in the coupling of a system code and a CFD code have been addressed in a previous NEAMS report [10], including data exchange method, driving mechanism, time synchronization scheme, and the selection of data for exchange. The coupling strategy between the System Analysis Module and the CFD code STAR-CCM+ [11] was derived and implemented based on these considerations and the characteristics of each code.

The multi-scale coupling capability has been demonstrated in the coupled SFR System Analysis Module and STAR-CCM+ code simulation of the ABTR PLOF transient. The details of the coupled code simulation can be found in Ref. [12] and [13]. The importance of the multi-resolution capability was demonstrated by the multi-dimensional flow and the formation of thermal stratification layers in the outlet plenum of the ABTR during the postulated transient, as seen in Figure 2.

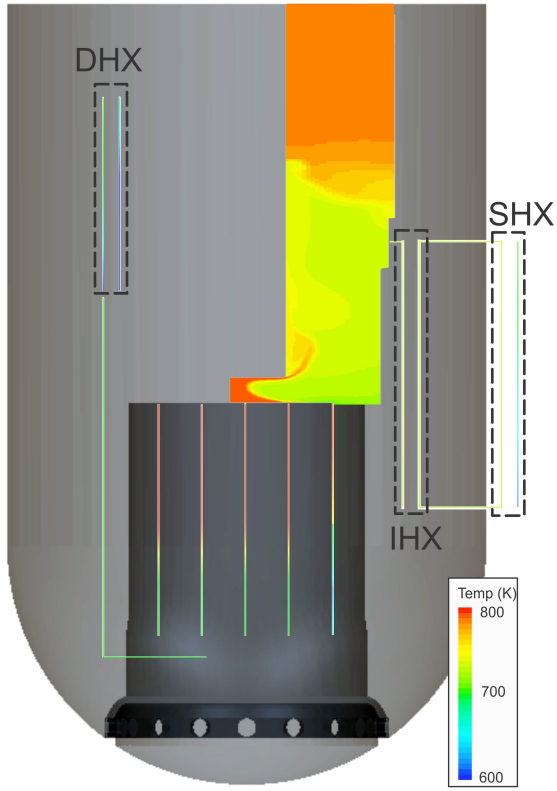

Figure 2: Temperature Distribution in a Coupled System and CFD Transient Simulation

2.4 Advantages over Current System Codes

Compared to current system codes, such as RELAP5, CATHARE and SAS4A/SASSYS-1, the SFR System Analysis Module represents a significant advance in physics models, numerical methods, and software designs for the system thermal-hydraulic simulation capabilities needed by these codes. A brief comparison between them is shown in Table 2.

Table 2. Key Features Comparison between Traditional System Tools and SFR System Analysis Module

	Relap-5, CATHARE, SAS4A/SASSYS-1, etc.	**SFR System Analysis Module**
Capacities	Extensive capabilities and knowledge after 40 years code development and user experience; Better for short transients with strong energy and momentum sources	Currently capabilities only include single-phase fluid flow and heat transfer, plus basic point kinetics model; Able to accurately model long transients with weak driving sources; multiple dimensional capabilities and additional physics available by coupling with external applications
Software design	Fortran 77, 90/95 Procedural/Modular programming	C++ OOP, Generic Programming, Modern software design
Numerical methods	Customized, semi-implicit 1st order accuracy in time and space (in theory), finite-difference "like" discretization, serial	Based on parallel nonlinear solvers (PETSc), Jacobian-free Newton-Krylov nonlinear solver (JFNK); fully coupled multiphysics;* 2nd order in both time and space; continuous FEM;
V&V	Primarily validation	Both verification and validation; SAS4A/SASSYS-1 validation data plus additional available data
Maintenance and Improvements	Significant efforts	Easy to develop, maintain, and improve, scalable; easy to couple with other modern codes

*: Operator split method could be implemented as solver or preconditioner once the MOOSE support is ready.

3 An advanced One-D FEM Flow Model and Verification

3.1 Governing Equations

The transport equations for one-dimensional, single-phase flow can be described by the following set of PDEs. The mass, momentum, and energy conservation equations are closed by the equation of state for the fluid.

$$\frac{\partial \rho}{\partial t} + \frac{\partial (\rho u)}{\partial z} = 0 \tag{1}$$

$$\frac{\partial (\rho u)}{\partial t} + \frac{\partial (\rho u u)}{\partial z} = -\frac{\partial p}{\partial z} - \rho g - \nabla \cdot \bar{\bar{\tau}} \tag{2}$$

$$\frac{\partial (\rho H)}{\partial t} + \frac{\partial (\rho u H)}{\partial z} = \nabla (k \nabla T) - \nabla q_r" + q''' + \frac{Dp}{Dt} + \phi \tag{3}$$

$$\rho = \rho(p, T) \tag{4}$$

Where, t: time; z: the axial coordinate in flow direction; ρ: the coolant density; u: velocity; g: the acceleration due to gravity; p: pressure; $\bar{\bar{\tau}}$: shear stress; T: temperature; E: internal energy; H: enthalpy, and $H = E + p/\rho$; k: fluid thermal conductivity; q_r'': radiation heat flux; q''': volumetric internal heat source; ϕ: source terms due to external forces, $\phi = -v \cdot (\nabla \cdot \bar{\bar{\tau}} + \rho g)$, including frictional dissipation, gravity, etc.

The shear stress in the momentum equation can be simplified using the friction coefficient. The energy equation can be simplified by neglecting the energy variation due to fluid conduction, radiation heat, thermal expansion, and the source terms due to external forces. After the simplifications and applying the continuity equation into the momentum and energy equations, the set of governing equations can be written in the conservative form (Eq.-5) or in the non-conservative form (Eq.-6).

$$\begin{aligned} &\frac{\partial \rho}{\partial t} + \frac{\partial (\rho u)}{\partial z} = 0 \\ &\frac{\partial (\rho u)}{\partial t} + \frac{\partial (\rho u u + p)}{\partial z} = -\rho g - \frac{f}{D_e}\frac{\rho u |u|}{2} \\ &\frac{\partial (\rho \mathrm{H})}{\partial t} + \frac{\partial (\rho u \mathrm{H})}{\partial z} = q''' \\ &p = p(\rho, \rho u, \rho E) \text{ or } \rho = \rho(p, T) \end{aligned} \tag{5}$$

In which f: the friction coefficient; D_e: equivalent hydraulic diameter. When considering the convection heat flux from solid surface q_s'', $q''' = \frac{q_s'' P_h}{A_c}$, where P_h and A_c respectively denote heated perimeter and cross-sectional area of the coolant channel.

$$\frac{\partial \rho}{\partial t} + \frac{\partial(\rho u)}{\partial z} = 0$$

$$\rho \frac{\partial u}{\partial t} + \rho u \frac{\partial u}{\partial z} = -\frac{\partial p}{\partial z} - \rho g - \frac{f}{D_e}\frac{\rho u|u|}{2} \tag{6}$$

$$\rho C_p \frac{\partial T}{\partial t} + \rho C_p u \frac{\partial T}{\partial z} = q'''$$

$$\rho = \rho(p, T)$$

In which C_p: the specific heat, $C_p = \frac{\partial H}{\partial T}$.

To solve the above set of PDEs, two out of three variables of density, pressure, and temperature (or total energy) must be selected as the state variables, along with the velocity (or mass flux) to compose the three state variables for the system of equations. Two common approaches used in the literature include: (1) primitive variable (or pressure) based formulation, in which the state variables are pressure (p), velocity (u), and temperature (T); and (2) conservative variable (or density) based formulation that uses density (ρ), momentum (ρu), and total energy (ρE) as the state variables.

Historically, the pressure-based approach was developed for low-speed incompressible flows, while the density-based approach was originally designed for high-speed compressible flows. Both methods have been extended and reformulated to solve and operate for a wide range of flow conditions beyond their traditional or original intent. The use of conservative variable ($\rho, \rho u, \rho E$) as independent variables would require the pressure to be calculated from equation of state (EOS). However, this approach may increase the difficulties in code convergence for applications of incompressible or nearly incompressible liquid flows, since small perturbations in ρ (density) or ρE (volumetric total energy) would cause significant changes in pressure. To use Newton-type nonlinear solvers, the $\partial p/\partial \rho$, $\partial p/\partial \rho u$, $\partial p/\partial \rho E$, $\partial T/\partial \rho$, $\partial T/\partial \rho u$, $\partial T/\partial \rho E$ terms are required for constructing the Jacobian matrix. Even if a matrix-free method is used, these derivative terms may still be needed for the preconditioning matrix. The existence of these terms significantly increases the difficulties in deriving the Jacobian or preconditioning matrix and may cause convergence problems when using real fluid EOS.

Although the conservative variable based formulation has the advantages in the applications of compressible flow, such as the capability to capture shock waves, the primitive variable based FEM formulation is more suitable for incompressible or nearly incompressible flows, such as the fluid flow in SFRs, LFRs, or FHRs. With the primitive variable approach, using the integral equations in the conservative form (Eq.-5) will still ensure the conservation laws of the fluid equations. Hence, a primitive variable based formulation was developed in this work for SFR system analysis applications.

The variation of coolant density is obtained from a pressure-temperature state relation as:

$$\delta\rho = \frac{\partial\rho}{\partial h}|_p \delta h + \frac{\partial\rho}{\partial p}|_h \delta p = \xi\delta h + \eta\delta p$$

$$\frac{\partial\rho}{\partial t} = \xi\frac{\partial T}{\partial t} + \eta\frac{\partial p}{\partial t} \tag{7}$$

$$\frac{\partial\rho}{\partial z} = \xi\frac{\partial T}{\partial z} + \eta\frac{\partial p}{\partial z}$$

And for incompressible but thermally expandable flow, $\frac{\partial\rho}{\partial t} = \xi\frac{\partial T}{\partial t}$ and $\frac{\partial\rho}{\partial z} = \xi\frac{\partial T}{\partial z}$. These formulas are needed for the primitive variable based formulation since density is a dependent variable.

3.2 SUPG/PSPG Stabilization and the Solution Scheme

Finite element analysis of incompressible flows requires stabilization to avoid the potential for numerical instabilities. The presence of advection terms (first order terms) in the governing equations can result in spurious node-to-node oscillations, as the unphysical pressure oscillation in a straight pipe shown in Figure 3. Stabilization methods successfully applied in structure problems, where no convection is present, may totally fail when they are applied to convection-dominated problems, as they occur frequently in fluid mechanics. This is particularly the case with Bubnov-Galerkin methods, which are weighted residual methods where the test functions are set equal to the shape functions [14]. The role of convection in differential equations can be defined by the Peclet number or Reynolds number. The higher these numbers are, the more dominant the convection term and the stronger the oscillations.

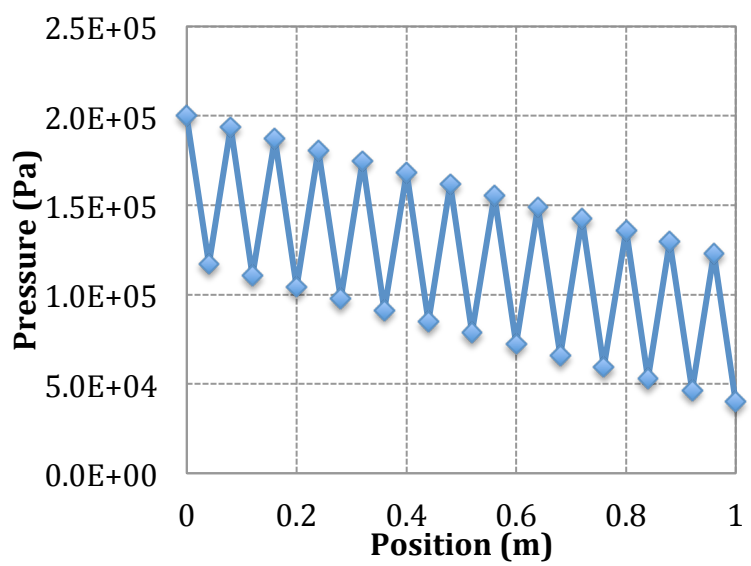

Figure 3: An example of non-physical (numerical) pressure oscillation

The same situation can also be found in the finite difference context. There, the same problem with oscillations occurs when using central differences for the advective operator. In finite difference methods, it is well known that upwind differencing on the convective term does not show oscillatory solutions, but introduces over-diffusive results. A simple Taylor series analysis proves that upwinding is only first order accurate, in contrast to the second order accurate, but oscillatory, central differences. This analysis also elucidates that upwinding can also be interpreted as central differences plus artificial diffusion. Thus, the "right" combination of central and upwind differences may introduce the optimal amount of artificial diffusion, which leads to accurate and oscillation-free solutions [13].

Starting in the 1970s a large number of FEMs arose with different ideas to include the up-wind effect in finite element analyses. The Streamline-Upwind/Petrov-Galerkin (SUPG) method, introduced from Brooks and Hughes in Ref. [13] can be considered as the first successful stabilization technique to prevent oscillations in convection-dominated problems in the FEM. The main concept is to introduce artificial diffusion in the streamline direction only, interpreted as a modification of the test function of the advection terms, and to enforce consistency, such that this modified test function is applied to all terms of the weak form. The term "artificial diffusion" is not fully applicable any longer, because the stabilized weak form cannot be manipulated such that only a diffusion term is extracted. The exact solution of the original problem still satisfies the SUPG stabilized weak form.

Considering a PDE of the general form,

$$Lu = f \tag{8}$$

where L is any differential operator. The SUPG weak form of the problem is:

$$\int_{\Omega} w^* * (Lu - f) d\Omega = 0 \tag{9}$$

The standard Bubnov-Galerkin test functions w are modified by a streamline upwind perturbation of the kind

$$w^* = w + \tau * L_{adv} w = w + \tau * \nabla w \tag{10}$$

Where L_{adv} is the advective part of the whole operator L, and τ is the stabilization parameter that weights the perturbation. Note that the perturbation is multiplied with the residual form of the differential equation. Thereby, consistency is fulfilled from the beginning in that the exact solution also fulfills the stabilized weak form exactly. It is because of this property of the SUPG stabilization (and the PSPG stabilization mentioned later) that numerical oscillations are prevented without introducing excessive numerical diffusion, and therefore without compromising the accuracy of the solution.

The Pressure-Stabilizing/Petrov-Galerkin (PSPG) method is a common technique used for the stabilization of the Stokes equations. For Stokes equations:

$$\text{Continuity equation: } \nabla \cdot u = 0$$
$$\text{Momentum equation: } \nabla \cdot \ (\nu \nabla \cdot u + p) = f \tag{11}$$

The PSPG stabilization term, similar to that of the SUPG, consists of a perturbation $\tau \nabla q$ multiplied with the residual of the momentum equation, but it is added to the weak form of the continuity equation.

$$\int_{\Omega} q * (\nabla \cdot u) d\Omega + \int_{\Omega} \tau \nabla q \ * (\nabla \cdot (\nu \nabla \cdot u + p) - f) d\Omega = 0 \tag{12}$$

In mixed convection-dominant problems, such as the incompressible Navier-Stokes equations with high Reynolds number, SUPG and PSPG (called herein SUPG/PSPG) stabilization have to be applied to obtain satisfactory results. It should be mentioned that the PSPG stabilization parameter does not necessarily have to be identical with the SUPG stabilization parameter. In this work, the weak forms of the stabilization schemes for incompressible flow are derived as:

$$\begin{aligned}
&\left(\frac{\partial \rho}{\partial t} + \frac{\partial(\rho u)}{\partial z},\ \psi\right) + \left(\frac{\partial \rho}{\partial t} + \rho u \frac{\partial u}{\partial z} + \frac{\partial p}{\partial z} + \rho g + \frac{f}{D_e}\frac{\rho u|u|}{2},\ \tau_{PSPG} * \nabla \psi\right) = 0 \\
&\left(\frac{\partial \rho u}{\partial t} + \frac{\partial \rho u u}{\partial z} + \frac{\partial p}{\partial z} + \rho g + \frac{f}{D_e}\frac{\rho u|u|}{2}, \psi\right) \\
&\qquad + \left(\rho \frac{\partial u}{\partial t} + \rho u \frac{\partial u}{\partial z} + \frac{\partial p}{\partial z} + \rho g + \frac{f}{D_e}\frac{\rho u|u|}{2}, \tau_{SUPG} * \nabla \psi\right) = 0 \\
&\left(\frac{\partial \rho \mathrm{H}}{\partial t} + \frac{\partial \rho u H}{\partial z} - q''', \psi\right) + \left(\rho C_p \frac{\partial T}{\partial t} + \rho C_p u \frac{\partial T}{\partial z} - q''', \tau_{SUPG} * \nabla \psi\right) = 0
\end{aligned} \tag{13}$$

in which ψ is the test function; τ_{PSPG} and τ_{SUPG} are the stabilization parameters that weights the perturbations; and $(f, \psi) = \int_{\Omega} \psi * f \, d\Omega$, is an expression of the volume integral. Note that the regular residuals of all conservation equations are calculated based on the conservative form while the stabilization terms are calculated based on the non-conservative form. This formulation not only strictly ensures the conservation laws, but also is easy to implement. A review of stabilized finite element formulations for incompressible flow, including the SUPG and PSPG schemes, can be found in Ref. [15].

The above formulation of the finite element method has been implemented in the SFR System Analysis Module, which is based on solving all systems in a fully coupled manner (i.e. all the unknowns are solved altogether in a large nonlinear system). The full coupling between different physics is achieved through the Jacobian-Free Newton Krylov (JFNK) method [16]. The JFNK method is a multi-level approach in solving large nonlinear systems, using outer Newton's iterations (nonlinear solver) and inner Krylov subspace methods (linear solver). The concept of "Jacobian-free" is proposed since deriving and assembling such large Jacobian matrices could be difficult and expensive. However, in most applications, the Krylov

subspace methods require preconditioning to be efficient. Although the JFNK method is used, the entries to the Jacobian matrix are still derived and implemented for the preconditioning purpose, since other preconditioning approaches have not worked well so far. The execution speed of the code strongly depends on the number of nonlinear (Newton) and linear (Krylov) iterations. The JFNK method has become an increasingly popular option for solving large nonlinear equation systems arising from multi-physics problems over the last 20 years, and has branched out into a number of different disciplines. The details of the JFNK method and some preconditioning techniques can be found in Ref. [16].

3.3 Verification Tests

The primitive variable based finite element fluid model has been implemented in the SFR System Analysis Module and verified by many problems. Density wave propagation, steep gradient problems, discharging between tanks, and the conjugate heat transfer in a heat exchanger are presented in this section.

3.3.1 Density Wave Oscillations

One challenging problem for traditional system codes, such as TRACE and RELAP-5, is to accurately model the wave oscillation or the sudden disturbance of the system without any numerical instability and numerical diffusion concerns due to their first-order approximations of the differential equations in both time and space.

An example of density wave propagation is presented here in a pipe flow problem. The inlet temperature of a one-meter pipe oscillates following a sinusoidal distribution, $T_{in}(t) = 628 + 100 * sin\,(\pi t)$; the inlet velocity is fixed, $u_{in}(t) = 0.5\,m/s$; and the initial pipe temperate is at 628 K. The transient responses of the wave propagation are shown in Figure 4, where the code predictions agreed very well with the analytical solutions. This is because the second order numerical accuracy in both space and time are implemented. In the finite element formulation, using piecewise linear shape functions for the state variables (pressure, velocity and temperature) assures the second order accuracy in space with both uniform and nonuniform discretization . Multiple time-integration schemes are available for the SFR System Analysis Module. The second-order backward differentiation (BDF2) scheme used in this analysis is second-order accurate in time. If a first-order time integration scheme were used, numerical damping or diffusion would occur, as shown in Figure 5.

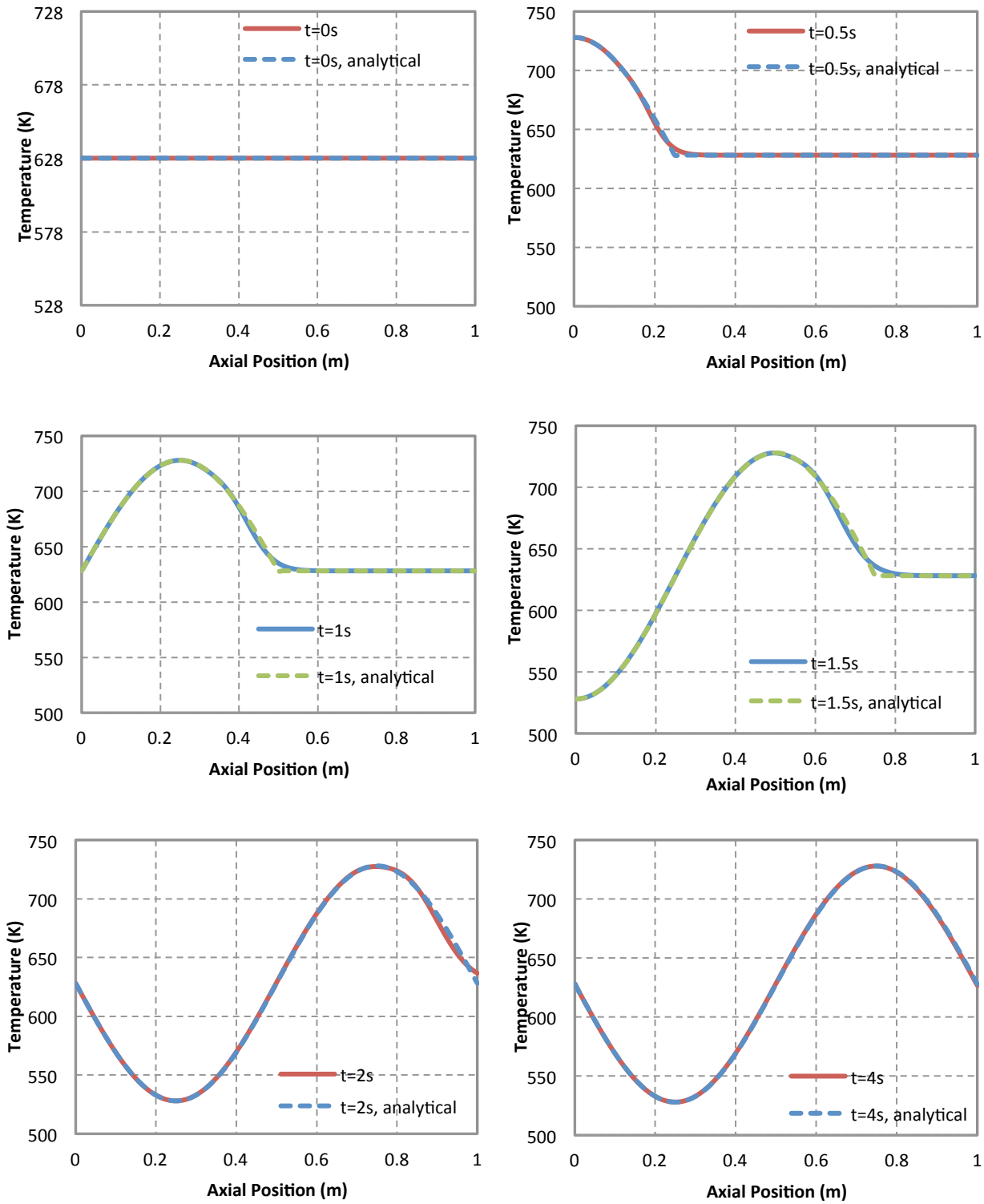

Figure 4: Transient responses of the pipe under inlet temperature oscillation, BDF2

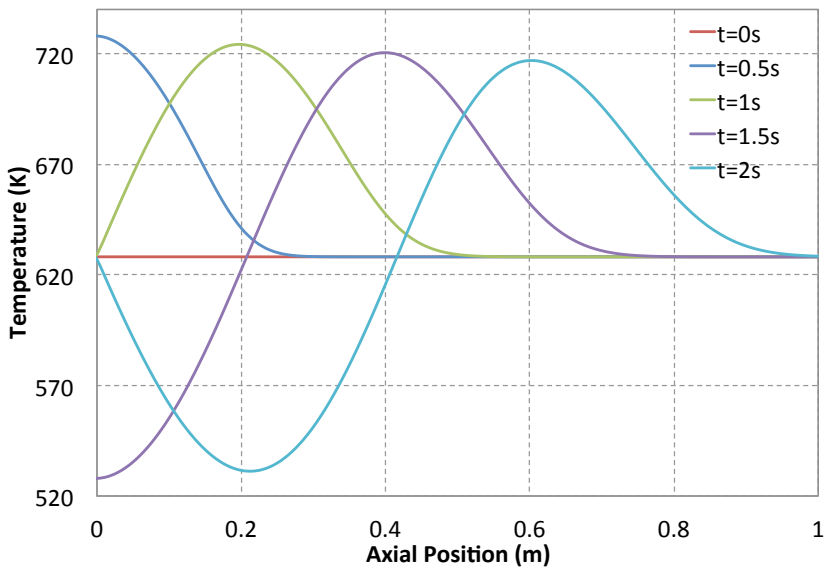

Figure 5: Damped temperature wave under inlet temperature oscillation, backward Euler

3.3.2 Steep Gradient Problems

A challenging problem, generally true for all types of numerical analyses, is the modeling of a non-continuity (steep gradient). Since the continuous finite element analysis is used in the SFR System Analysis Module, its capability to model steep gradient problems needs to be examined.

A steep gradient problem is tested again in a simple vertical pipe flow. The inlet temperature of the pipe follows a step function:

$$T_{in}(t) = \begin{cases} 628\ K, & if\ t \leq 0 \\ 728\ K, & if\ t > 0 \end{cases} \tag{14}$$

The inlet velocity is fixed: $u_{in}(t) = 1\ m/s$. The transient responses of the temperature step change are shown in Figure 6. The smoothing of the temperature gradient over time is clearly observed.

A similar steep gradient problem is tested with an inlet temperature pulse, in which the pipe inlet temperature follows

$$T_{in}(t) = \begin{cases} 628\ K, & if\ t > 0.1\ or\ t < 0 \\ 728\ K, & if\ 0 \leq t \leq 0.1 \end{cases} \tag{15}$$

The inlet velocity is fixed: $u_{in}(t) = 1\ m/s$. The transient responses of the temperature step change are shown in Figure 7. The smoothing of the temperature gradient is again observed. However, the smoothing shown in Figure 6 and Figure 7 can be deemed acceptable because: (1) no numerical overshooting is observed; (2) some physical diffusions (molecule diffusion, turbulence, conduction) are real, but commonly neglected in the 1-D flow formulation; (3) further refining the mesh would reduce the smoothing or damping.

Another steep gradient problem is tested with the step change of the inlet pressure of the pipe, as:

$$P_{in}(t) = \begin{cases} 1.0\times10^5\ Pa, & if\ t \le 0 \\ 2.0\times10^5\ Pa, & if\ t > 0 \end{cases} \tag{16}$$

The outlet pressure is fixed at $P_{out}(t) = 1.5\times10^5\ Pa$. The transient response of the flow velocity is shown in Figure 8. The flow velocities across the pipe responded simultaneously to the pressure step change. The flow reverses its direction after approximately 0.2 seconds and then stabilized at a new steady state. The transient response of the pressure step change is well captured by the developed FEM flow model. The code predictions of the velocities at the initial and final steady states agree very well with analytical solutions. Note that the differences in the absolute magnitudes of the initial and final steady-state velocities are due to gravity.

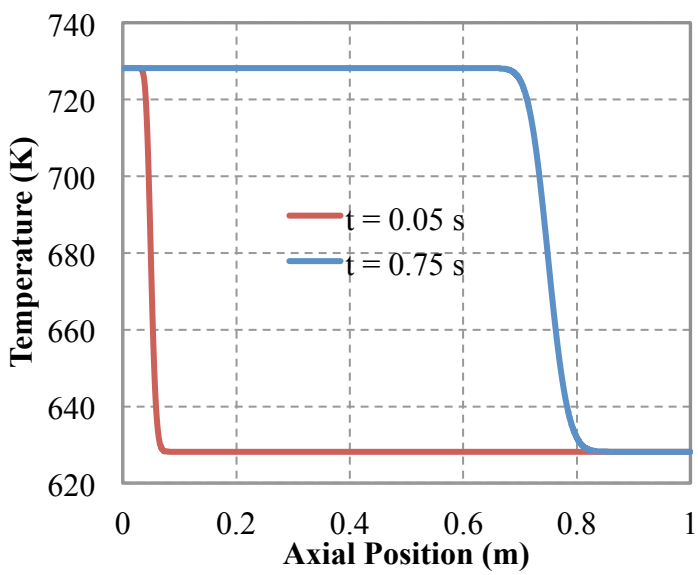

Figure 6: Smoothing of steep gradient during a temperature step change transient

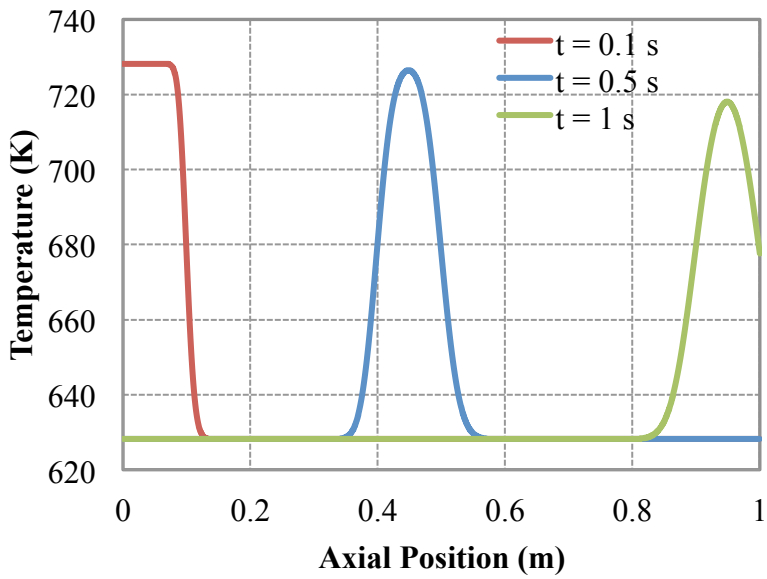

Figure 7: Smoothing of steep gradient during a temperature pulse transient

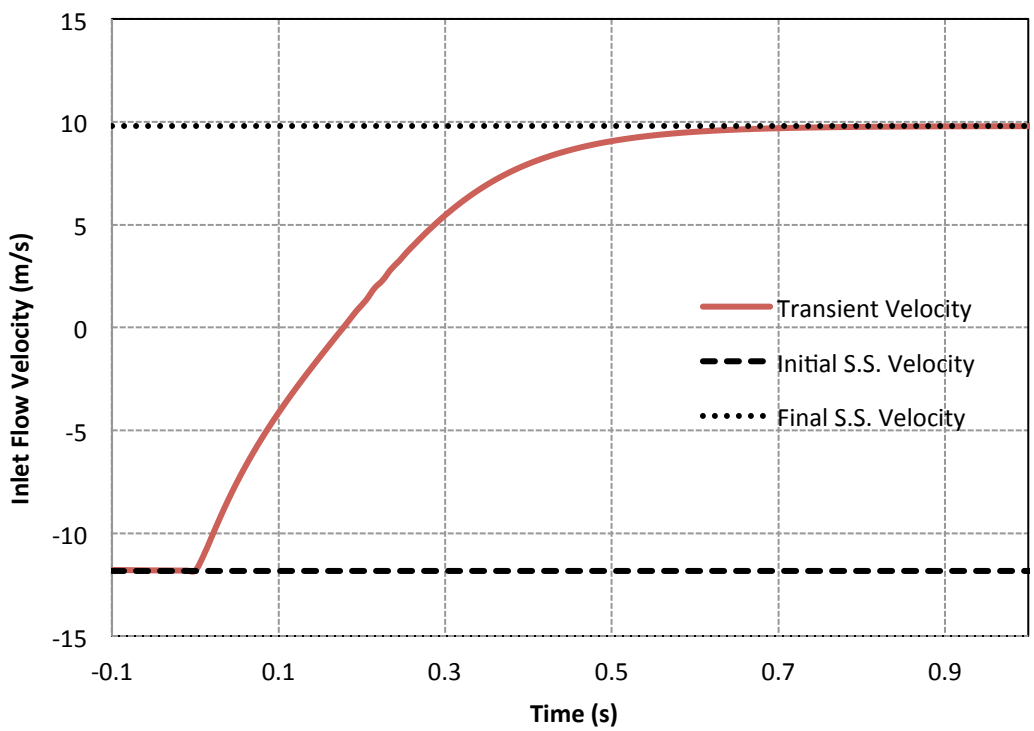

Figure 8: Flow velocity response during a pressure step change transient

3.3.3 Tank Discharge Problem

A tank discharge problem is modeled to examine the applicability of the code to a wide range of operating conditions during a transient. In this test, two liquid pools are connected through a valve (opens at $t = 0\ s$) and a pipe. The two pools share a common cover gas, but have different initial liquid levels and temperatures. The transient response of the tank discharge test is shown in Figure 9. It is confirmed the flow reversal is well captured, and the code performed very well (without any numerical instability problems) for a very wide range of flow conditions (from over 100 kg/s to less than 0.1 kg/s). Note that the cover gas and pool dynamics is also modeled in the code as 0-D components, but not elaborated in this paper.

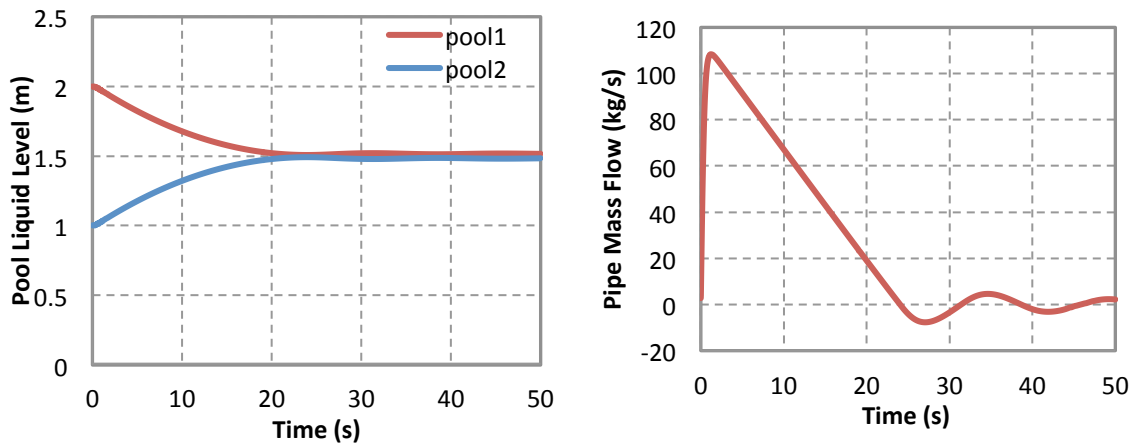

(a) Liquid level (b) Mass Flow

Figure 9: Transient response of the tank discharge test

3.3.4 Conjugate Heat Transfer Problems

An example of conjugate heat transfer in a counter-current heat exchanger is also examined, in which the operating condition of the intermediate heat exchanger (IHX) in the ABTR is used. The inlet temperatures are 783 K and 606 K for the primary and secondary pipes. The mass flow rates are also fixed at 1264 kg/s and 1259 kg/s for the two sides respectively. Because the flow rates are very close for the two sides, linear temperature distributions are expected for the two sides. The code predictions are shown in Figure 10, in which outlet temperatures of the two sides also agreed very well with the ABTR design values, 628 K and 761 K respectively.

Assuming constant heat transfer coefficients for both sides of the heat exchanger, constant wall thermal conductivity, and constant specific heat capacity of the fluid, the analytical solution of the temperature difference between the primary and secondary sides of the heat exchanger can be obtained from Eq. (17) using the thin-wall approximation for the tube wall.

$$ln\left(\frac{\Delta T(x)}{\Delta T(0)}\right) = -h_e P_h \left(\frac{1}{\dot{m}_p c_p} - \frac{1}{\dot{m}_s c_p}\right) x \tag{17}$$

In which ΔT is the fluid temperature difference between the primary and secondary sides, P_h is the heated perimeter, $\dot{m}_p$ and $\dot{m}_s$ are the mass flow rates of both sides, c_p is the specific heat capacity, and h_e is the effective heat transfer coefficient between the primary and secondary side. h_e is defined as:

$$h_e = \frac{1}{\frac{1}{h_p} + \frac{t}{k} + \frac{1}{h_s}} \tag{18}$$

In which, h_p and h_s are heat transfer coefficients in primary and secondary sides, respectively; and t and k are the thickness and thermal conductivity of the tube wall between primary and secondary sides, respectively. To obtain a clear exponential distribution of the temperature difference, the mass flow rate of the primary side in the above ABTR heat exchanger problem is reduced to half. The calculated and analytical fluid temperature differences between the primary and the secondary sides along the heat exchanger pipe are shown in Figure 11. The comparison indicates that the simulation results agree well with the analytical solution, with a maximum error of temperature difference less than 1 °K for the case with the coarsest mesh (with 10 elements for the 3.7 meter long heat exchanger).

A mesh convergence study has also been performed for this test problem. The number of axial pipe elements varies from 10, 20, to 40, while the radial element number of the wall remained unchanged at 2. The L2-Norms of the temperature differences are shown in Figure 12. It is clearly shown that the 2nd order accuracy has been achieved from the trend-line.

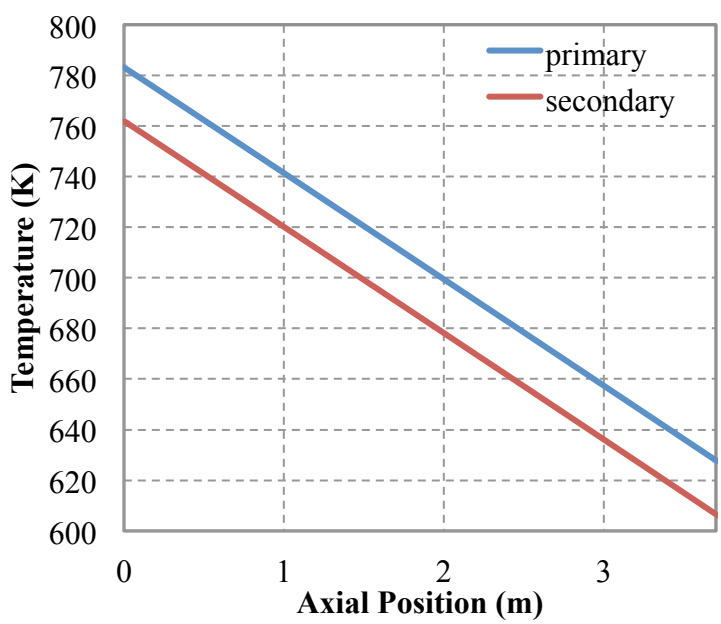

Figure 10: Temperature distribution of a counter-current heat exchanger

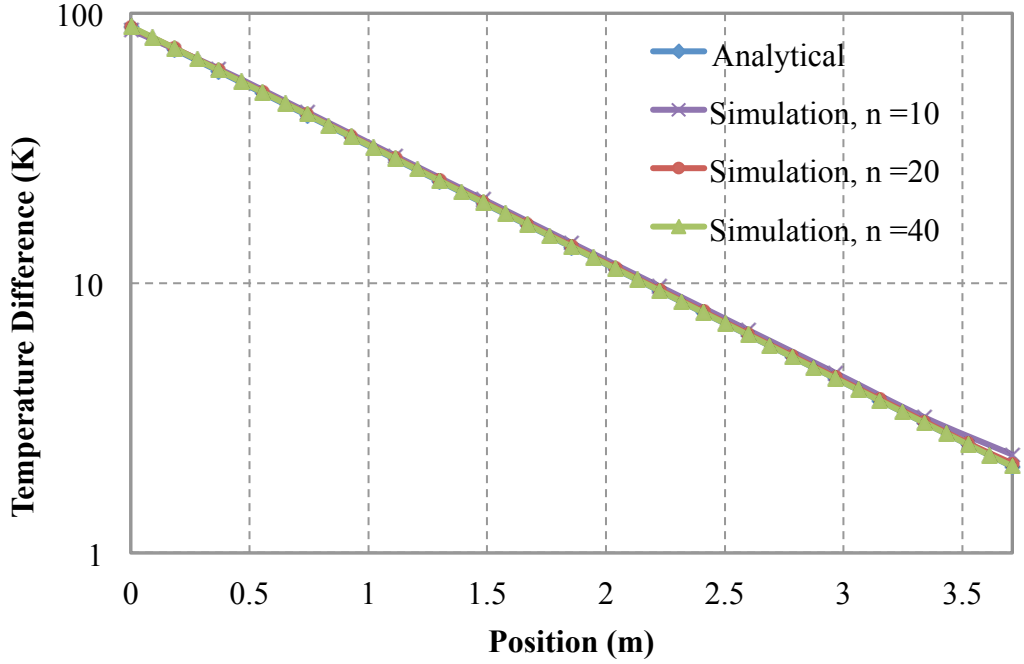

Figure 11: Temperature difference distribution of a counter-current heat exchanger

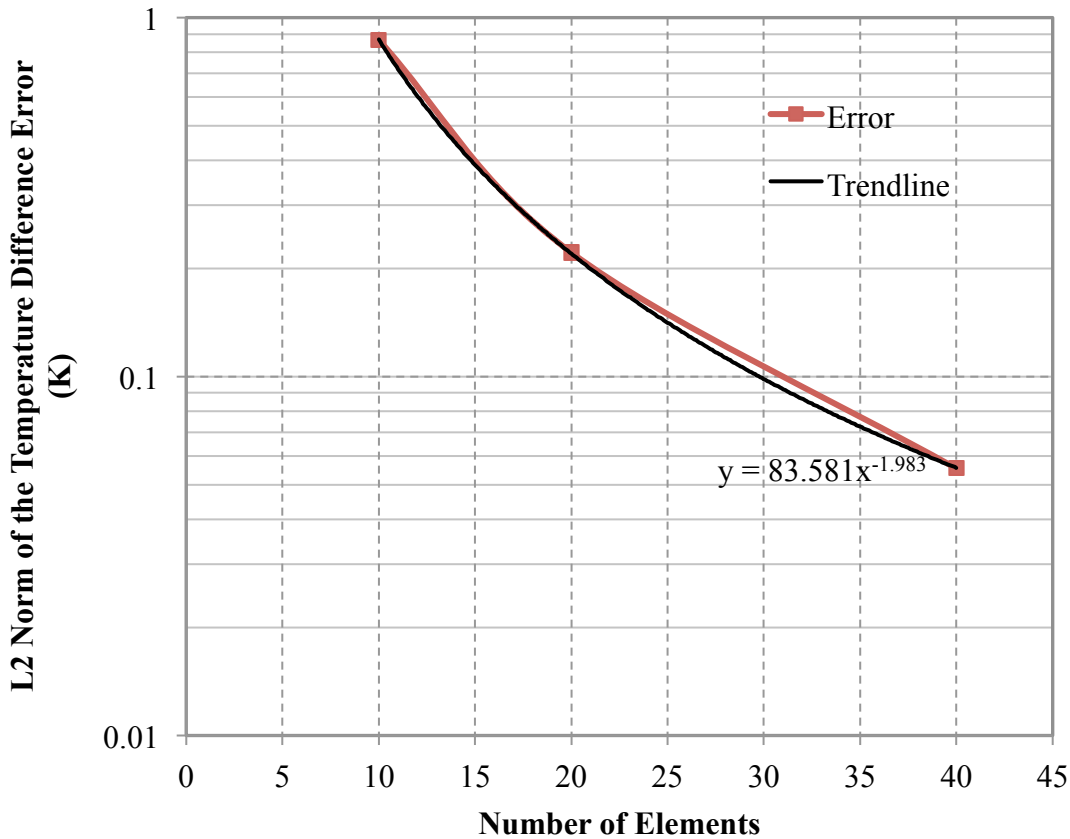

Figure 12: Spatial convergence study of a counter-current heat exchanger

4 Demonstration Simulation of ABTR

A typical SFR model based on the ABTR conceptual design was developed to examine the primary system simulation capabilities in the SFR Module in FY13. Both steady state and Protected Loss-Of-Flow (PLOF) transient were simulated. However, the effort in FY13 was focused on the development and performance of the ABTR simulations with Components using conservative variable based flow model.

In FY14, the focus shifted to develop integrated-physics components using the primitive variable based flow model. Results demonstrate that the primitive variable based flow model has superior convergence performance compared to the conservative variable based flow model for incompressible flows. The ABTR PLOF transient was used again as the test case.

4.1 Model Description

The detailed design parameters of the 250 MW pool-type ABTR can be found in Ref. [8]. The primary system is configured in a pool-type arrangement with the reactor core, primary pumps, intermediate heat exchangers, and direct reactor auxiliary cooling system heat exchangers all immersed in a pool of sodium coolant within the reactor vessel. Figure 13 shows the schematics of the ABTR model analyzed with the SFR Module. The primary coolant system consists of the downcomers (pump outlet and pump discharge), the lower plenum, the reactor core model, the upper plenum, and the intermediate heat exchanger. Five CoreChannels (flow channels with heat structure attached to each of them) were used to describe the reactor core. LiquidVolume components are used to represent the cold pool and the upper plenum. Both are connected to a CoverGas component. Different components are connected with Branches. The intermediate loop, the secondary loop, and the DRACS loop are modeled with great simplicities. Single-phase counter current heat exchanger models are implemented to mimic the function of the intermediate loop heat exchanger (IHX), DRACS heat exchanger (DHX), and secondary loop heat exchanger (SHX) to transfer heat among the primary, intermediate, secondary, and the DRACS loops. The geometric data of the multi-channel core and non-core components are Identical to the FY13 model.

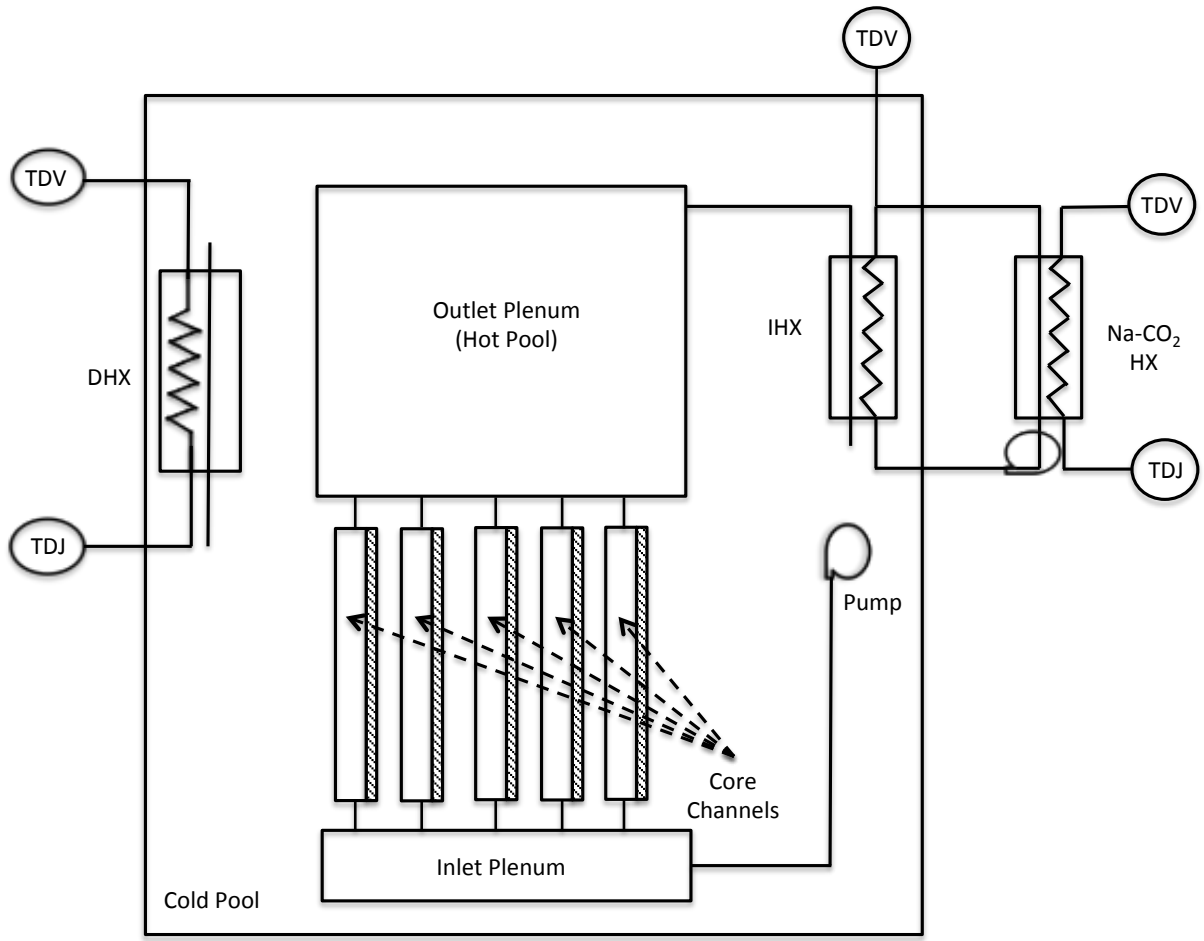

Figure 13: Schematics of the test ABTR model

4.2 Accident Sequences

The basic accident sequence analyzed here is the loss of normal power to the reactor and intermediate coolant pumps, with failure of the emergency power supplies. The result is a loss of forced flow in the primary and intermediate coolant circuits. In addition, it is assumed that heat removal at the power cycle heat exchanger ceases, so that the only heat removal path is through the emergency direct reactor auxiliary cooling system (DRACS). It is assumed that the reactor safety system acts as designed to insert control rods and reduce reactor power immediately to decay heat. This sequence is called the protected loss-of-flow (PLOF) accident.

The natural circulation DRACS is simply modeled as a heat exchanger in this demonstration problem. The inlet flow rate, inlet temperature, and outlet pressure are fixed at the secondary side as boundary conditions. The DRACS is designed to remove 0.5% of full power (1250 kW) at normal operating temperatures assuming failure of one DRACS unit.

The initial condition for the accident sequence is normal operation at full power and flow. With the loss of pumping power, flow in the primary circuit coasts down according to the spinning inertia of the pumps and motors. Following flow coast down, natural circulation flow is established. With the loss of power, forced flow in the intermediate coolant system is also lost. The intermediate heat transport system (IHTS) is alternately a heat sink or source in

the accident sequence, depending on its temperature and the primary system temperature at the intermediate heat exchanger. During the transient, flow in the IHTS may reverse, depending on transient temperature conditions.

In the PLOF sequence, the absence of normal shutdown heat removal through the reactor coolant system causes a slow system temperature rise following the reactor scram. This temperature increase occurs because the DRACS has insufficient heat removal capacity to overcome both the early decay heat production rate and the stored heat in the primary and intermediate systems. Eventually, the decay heat falls below the DRACS capacity, and the system temperature declines.

4.3 Simulation Results

Similar to the FY13 model, the reactor power and primary pump head history from SAS4A/SASSYS-1 simulation results, shown in Figure 14, were used throughout the simulated PLOF transient. The pump in the intermediate loop is assumed to have the same coast-down characteristics. Both pumps were assumed to completely stop at about 420s.

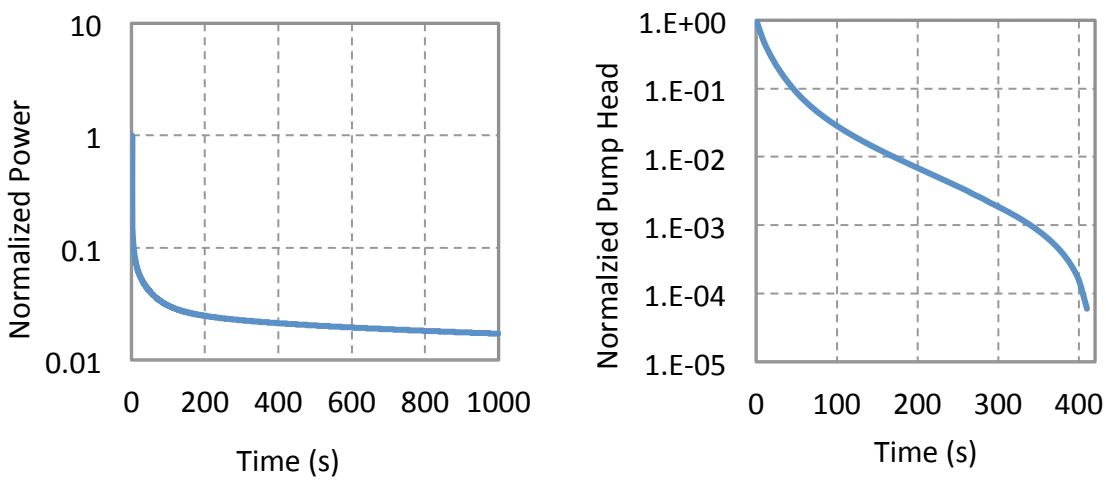

Figure 14: Normalized power and pump head history during PLOF

Results from analysis of the early part of the PLOF transient, during the pump coast down and transition to natural circulation, are shown in Figure 15-Figure 18. The normalized core power and flow rate are shown in Figure 15. This transient is initiated by a complete loss of forced coolant flow in the primary and intermediate loops. Both the primary and intermediate pumps are designed with sufficient flow inertia and cease operation at about 420 seconds after the start of the transient, leading to a transition to natural circulation. Immediately after the transient initiated, the reactor control system scrams the reactor, and then the reactor power is shortly reduced to decay heat. It is found in Figure 15 that the transition to natural circulation flow is very smooth. The power to flow ratio during the transient is actually always less than that of normal operating conditions, which assures that the safety of the reactor core during the transient. The core flow rate from FY13 simulation using components based on density based flow model is also shown in Figure 15. Almost identical flow rates were predicted for both pump coastdown phase and natural circulation phase. However, the simulation time for the 1000 second transient is significantly reduced from ~2 hours to ~8 minutes.

Figure 16 shows the flow velocities in all core channels during the transient. Similar behaviors are found, and the establishments of the natural circulation flows occur at the same time for all channels. Figure 17 shows the DRACS heat removal and the IHX heat removal rates. When the transient is initiated, the secondary side of the DRACS heat exchanger is assumed open immediately, permitting the DRACS to operate at its full capacity of removing 0.5% nominal power. As the cold pool temperature rises, DRACS heat removal capacity will increase accordingly. The loss of heat removal to the balance-of-plan is also assumed immediately after the transient by setting the flow in the secondary side of the secondary heat exchanger to zero. The heat removal rate from DHX is far less than the reactor decay heat power at the end of 1000 seconds. The DRACS heat removal capacity will equal the decay heat at about 5 hours into the transient. The heat removal rate from IHX is also shown in Figure 17. In spite of the very simplified model of the intermediate loop, it behaves alternately as a heat sink or source during the transient, depending on its temperature and the primary system temperature at the intermediate heat exchanger. This behavior is expected in the ABTR IHTS design for these transient boundary conditions.

The temperatures at the core inlet plenum, outlet plenum, and the cold pool are shown in Figure 18. Shortly after the transient, the only heat removal is through the DRACS. The rapid reactor power decrease due to the scram initially lowers the coolant and fuel rod temperatures in the core, and then the hot pool temperature. Then the drop in core flow due to the pump coast down and the increase of the core inlet temperature leads to the temperature rise in core and the hot pool. The cold pool temperature rises during the whole transient because the hot coolant continues entering the cold pool from the IHX outlet, and the heat removal from the DHX is not enough. This will continue until the DRACS heat removal capability becomes equal to the decay heat production, which will occur at about 5 hours. After that, the cold pool temperature will decrease as the whole system cools. The inlet plenum temperature response follows the similar trend of the cold pool temperature response, but with some delay.

This demonstration simulation focuses on the early stage of the PLOF transient. It is confirmed that major physics phenomena in the primary coolant loop during the transient can be well captured by the updated SFR System Analysis Module using the primitive-variable based flow model, and that the new flow model can significantly improve the code convergence speed for incompressible thermally expandable flow systems.

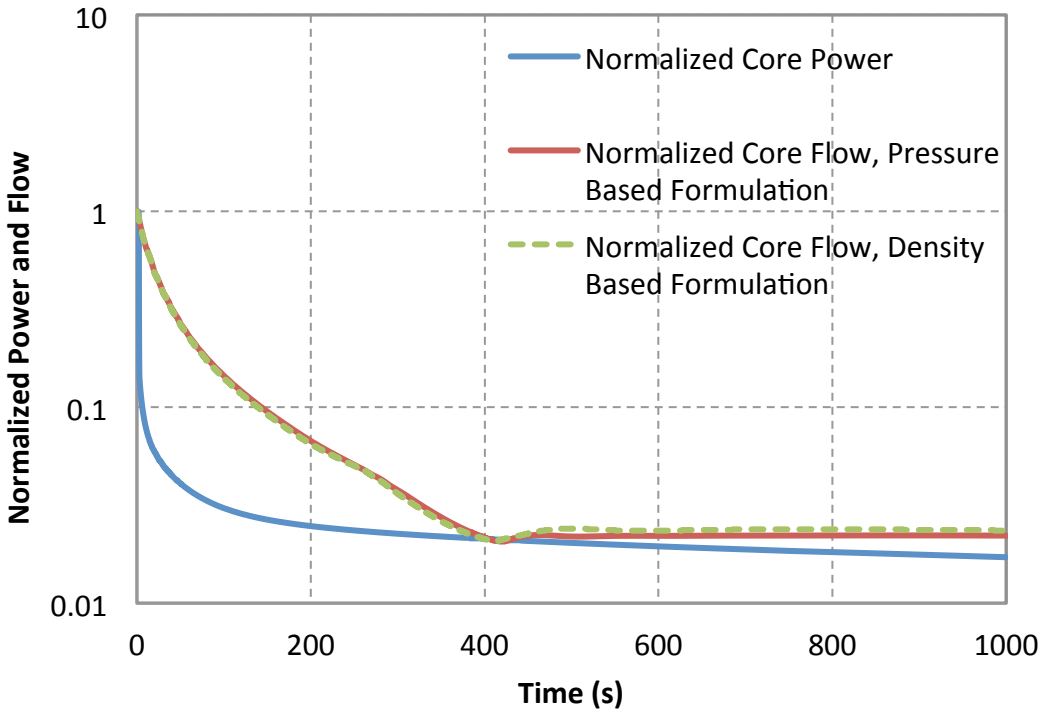

Figure 15: Normalized power and core flow during the PLOF transient

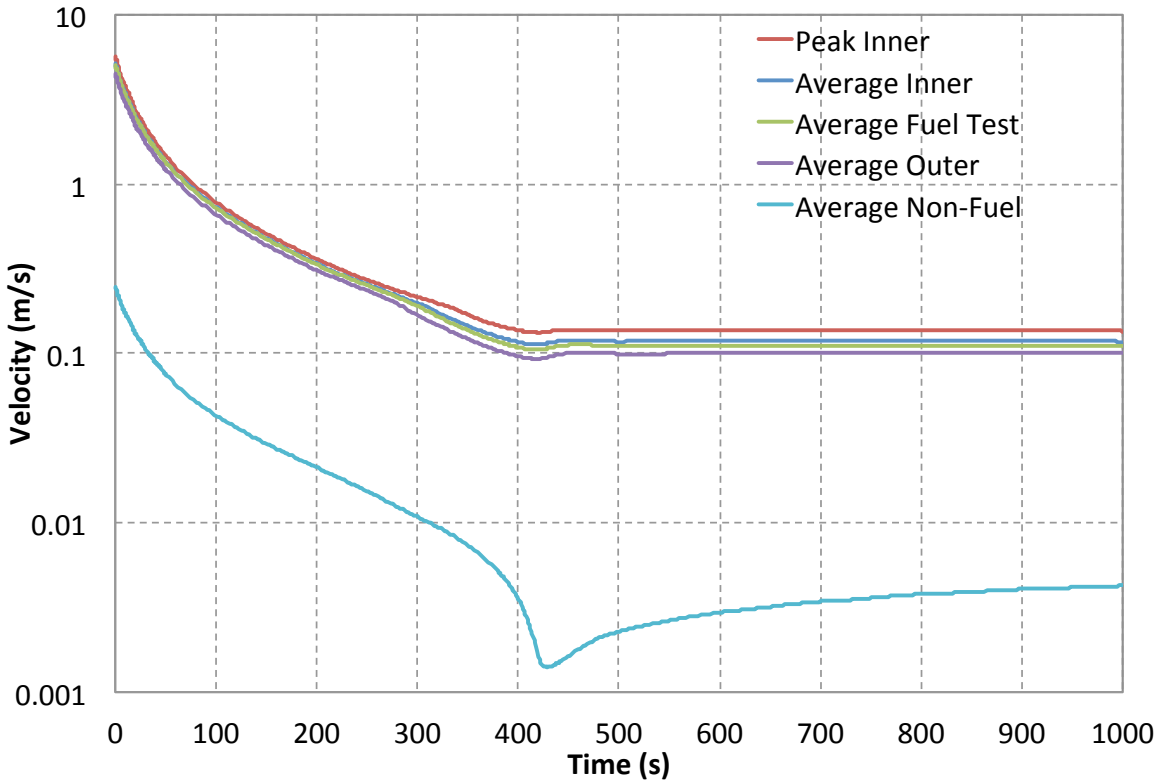

Figure 16: Core channel flow velocities during the PLOF transient

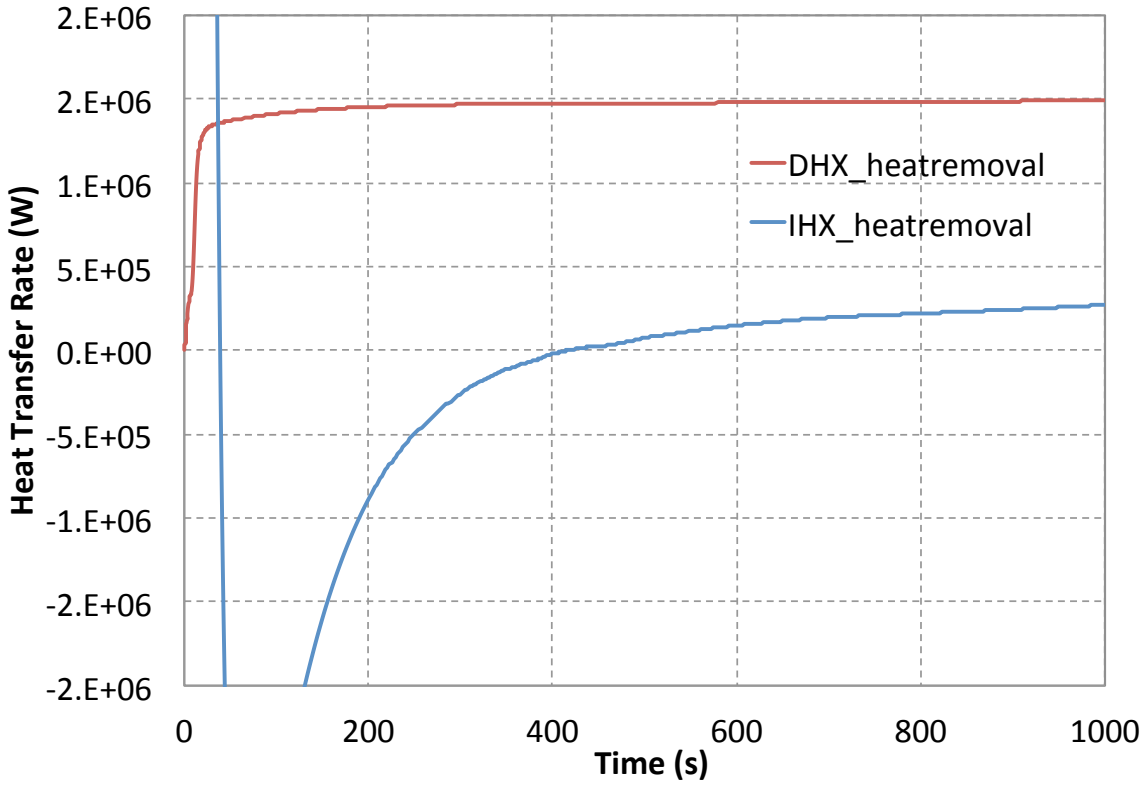

Figure 17: Heat removal rate from IHX during the PLOF transient

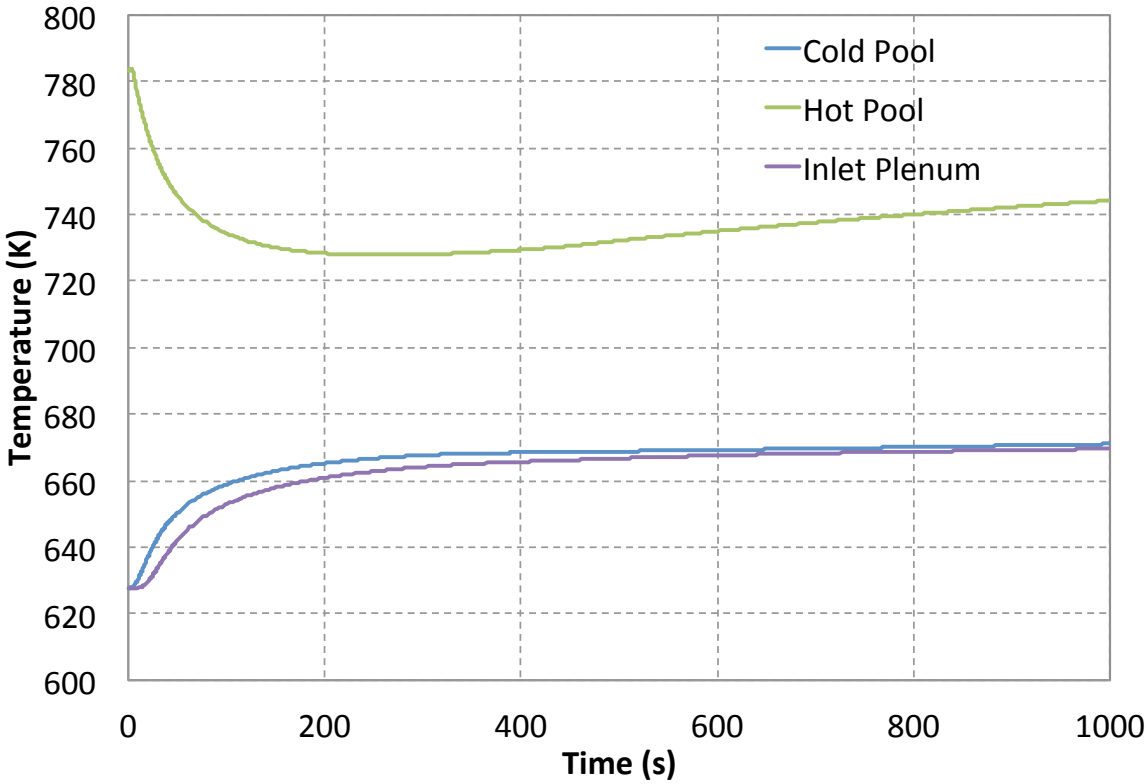

Figure 18: Pool temperatures during the PLOF transient

5 Simulation of EBR-II SHRT-17 Test

The EBR-II shutdown heat removal tests, carried out between 1984 and 1986, provide unique passive safety demonstration data that are critically important for validation of safety and systems analysis tools used to support fast reactor research and development programs in the U.S. and elsewhere. As a means of supporting international passive safety evaluation activities for fast reactors, two of the tests in the EBR-II Shutdown Heat Removal Test (SHRT) program have been selected as an IAEA coordinated research project (CRP) aimed at improvements in design and simulation capabilities of fast reactor analysis codes from around the world.

The benchmark specifications [17] for both the SHRT-17 protected and SHRT-45R unprotected loss-of-flow tests are available to CRP participants. However, some SFR specific reactivity feedback mechanisms, such as the radial and axial core expansion, control rod drive line expansion, etc., can not yet be modeled in the SFR System Analysis Module. Therefore, a simplified version of the protected SHRT-17 test will be modeled in which the power and pump head histories are defined as input to the model.

5.1 Model Description

SHRT-17 is a protected loss of coolant flow test starting at steady state operating conditions. The test involved a complete loss of all pumping power to the plant while operating at full power and flow, followed by a scram. The sodium coolant was under forced convection flow while the plant operated in steady state. Once the loss of flow transient began, forced convection flow continued while the pumps coasted down. After the pumps had stopped, the flow transitioned to natural circulation. The system then relied upon natural circulation to remove residual heat from the core.

The detailed design parameters of the 62.5 MW_{th} pool-type EBR-II can be found in Ref. [17]. The primary system is configured in a pool-type arrangement, with all major primary system components submerged in the primary tank. Two primary pumps drew sodium from this pool and provided sodium to the two inlet plena for the core. Subassemblies in the inner core and extended core regions received sodium from the high-pressure inlet plenum, accounting for approximately 85% of the total primary flow. The blanket and reflector subassemblies in the outer blanket region received sodium from the low-pressure inlet plenum. Hot sodium exited the subassemblies into a common upper plenum where it mixed before passing through the outlet pipe into the intermediate heat exchanger (IHX). The pipe feeding sodium to the IHX is referred to as the 'Z-pipe.' Sodium then exited the IHX back into the primary sodium tank before entering the primary sodium pumps again.

An EBR-II model, similar to the SAS4A/SASSYS-1 described in Ref. [17], has been developed for SHRT-17 benchmark simulation, as shown in Figure 19. To simplify the input preparation and for preliminary runs, flow leakages and the auxiliary pump are not modeled. All subassemblies are lumped into one of three core channels, namely Channel A (inner core), Channel B (outer core), and Channel P (peak) which receive 94.54%, 5.41%, and 0.4572% respectively of the total power of 57.3 MW prior to the transient. The three channels represent driver, reflector and blanket subassemblies, respectively with geometry information specified in Ref. [17]. The intermediate loop is modeled as the secondary side of the IHX, with the inlet flow and temperature through the transient provided as boundary conditions.

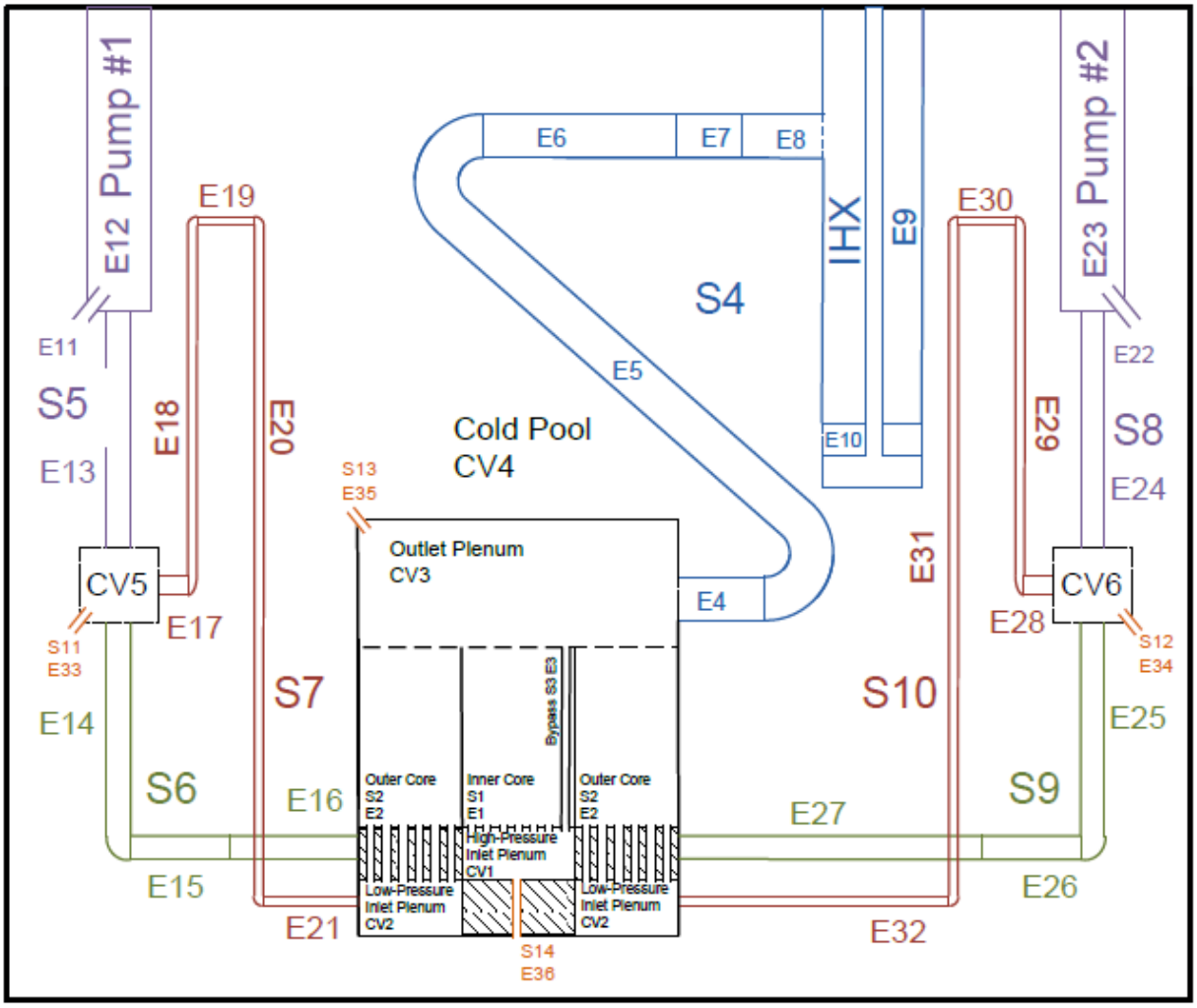

Figure 19: EBR-II Plant Model for SHRT-17 [17]

5.2 Simulation Results

Steady state simulation of the EBR-II model has been performed to assure the correct initialization of the operating conditions prior to SHRT-17 test. Orifice coefficients at the inlet plena are adjusted, and it is confirmed that the correct flow split (about 65.8 kg/s for the low pressure plenum and 389 kg/s for the high pressure plenum) has been achieved between the inner and outer inlet plena. The temperature distribution of the primary heat transport system is shown Figure 20, and selected locations are plotted in Figure 21. It is clearly shown that the model approaches steady state after 150 seconds while starting from uniform temperature and velocity conditions.

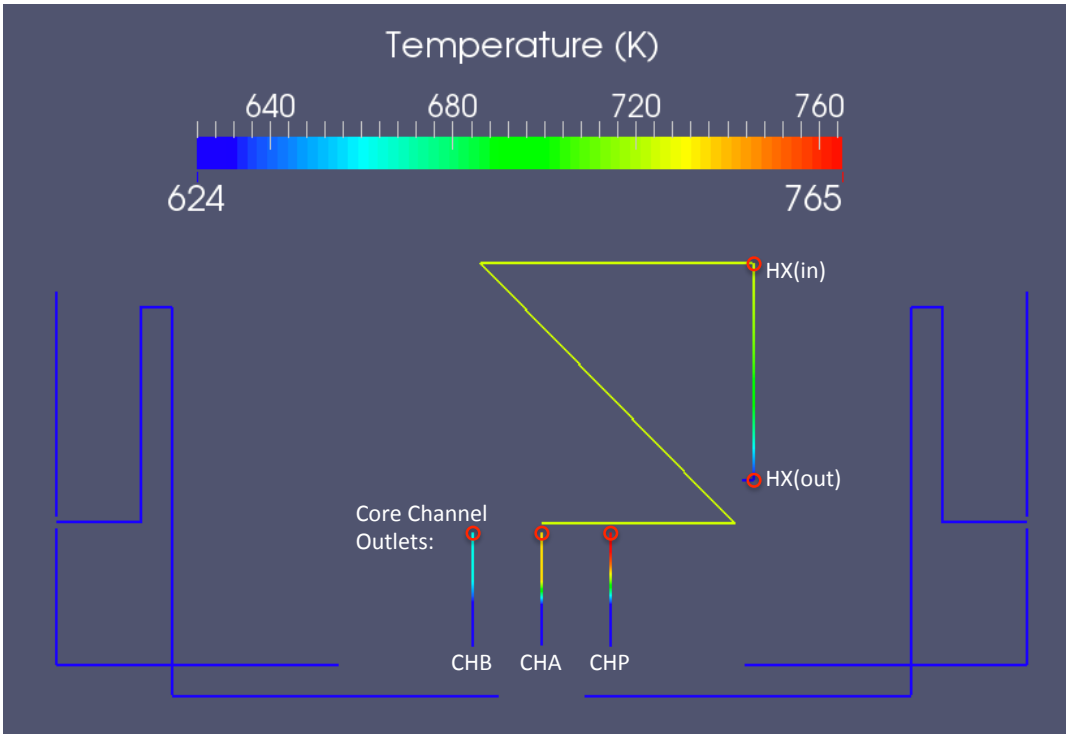

Figure 20: Temperatures distribution of EBR-II at steady-state

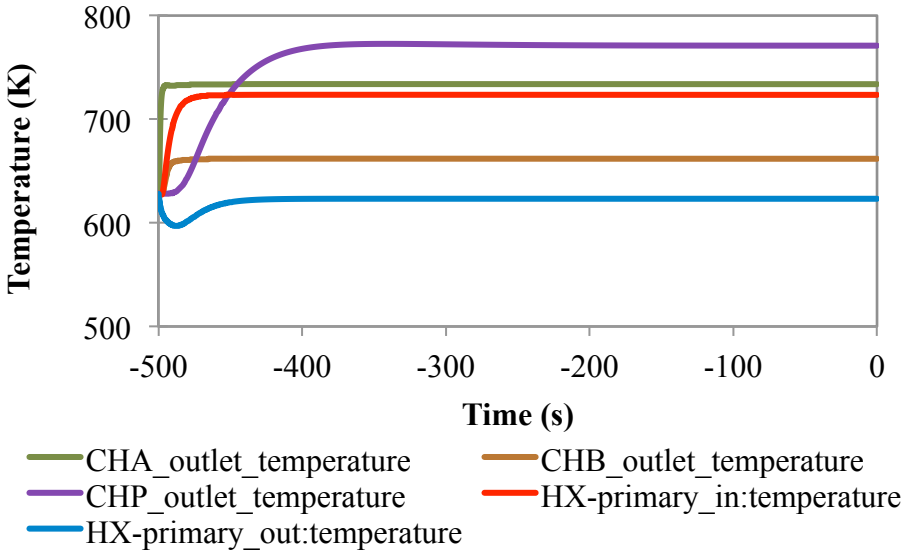

Figure 21: Temperatures response during steady state initialization

Similar to the ABTR PLOF simulation in Section 4, the reactor power and primary pump head histories are defined as input conditions for the EBR-II SHRT-17 model, as shown in Figure 22. Both pumps were assumed to completely stop at about 50 seconds.

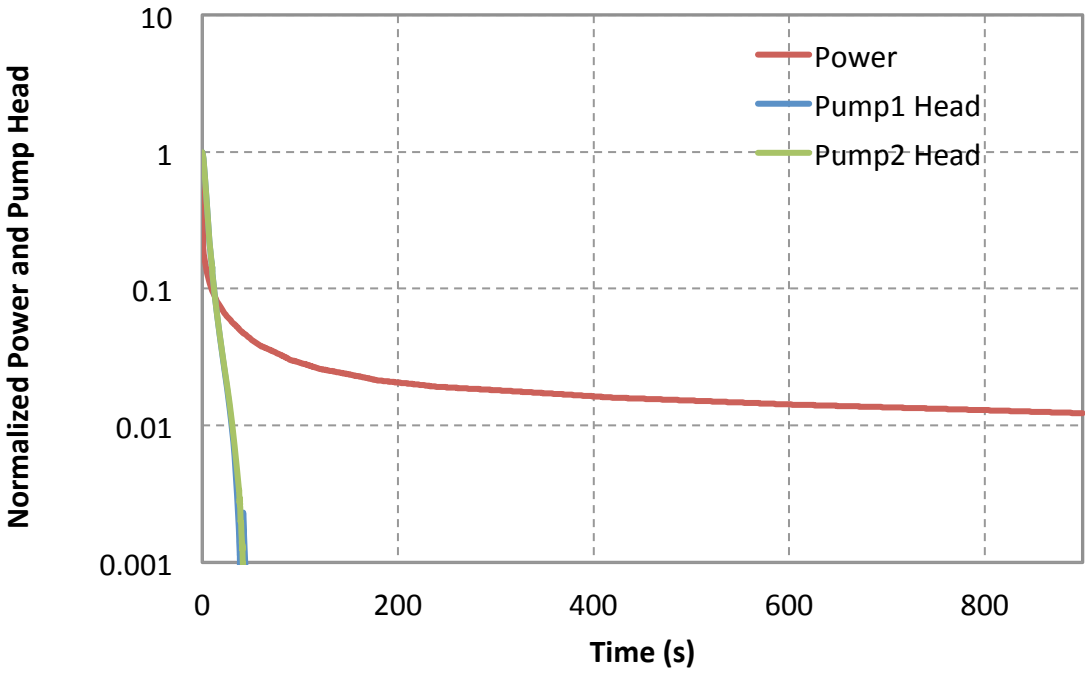

Figure 22: Normalized power and pump head history during SHRT-17 test

Simulation results of the SHRT-17 test are shown in Figure 23 - Figure 29. The normalized core power and flow rate are shown in Figure 23. This transient is initiated by a complete loss of forced coolant flow in the primary loop. The two primary pumps are designed with sufficient flow inertia and cease rotation at about 50 seconds after the start of the transient, leading to a transition to natural circulation. Immediately after the transient initiated, the reactor control system scrams the reactor, and then the reactor power is quickly reduced to decay heat. It is found in Figure 23 that the transition to natural circulation flow is very smooth. The transient response of the core flow in the simulation is similar to that from the experiment, although the magnitudes are slightly different. This is deemed acceptable because of all the simplifications used in the current EBR-II model. However, further investigations are needed to resolve or to better understand the causes of these differences.

The core outlet temperatures and upper plenum temperature are shown in Figure 24. The transient responses of the core outlet temperatures in the simulation are very similar to the experiment. The rapid reactor power decrease due to the scram initially lowers the core outlet and then the outlet plenum temperature. Then the drop in core flow due to the pump coast down and the increase of the core inlet temperature leads to the temperature rise in core and the hot pool. Once the natural circulation flow is fully established and because the IHX heat removal is higher than the core power, the core outlet temperatures start dropping again. It should be also noted that the thermal couples in the upper plenum were concentrated in specific locations and complex geometry and flow pattern existed in the EBR-II core outlet plenum. Therefore, the average value of these measurements are not the real average temperature of the core outlet plenum [18].

The IHX Inlet temperature response during the transient is shown in Figure 25. Very large differences are found between the code predictions and the measurements. Additionally, it is also found that the IHX inlet temperature is significantly lower than the core outlet

temperature. It has been suspected that there may be significant amount of heat losses through the Z-pipe between the core outlet plenum and the IHX. Therefore, another simulation is performed by considering the maximum Z-Pipe heat losses (ignoring the insulation and sodium gaps). The effects of the Z-Pipe heat loss can be observed from Figure 25-Figure 27. While the IHX inlet temperature is only 1.5 degree lower than the core outlet plenum temperature under steady state full flow conditions, the IHX inlet temperature is significantly affected by the Z-Pipe heat loss due to the longer transit time in the Z-Pipe under low flow transient conditions, as shown in Figure 26. However, it does not significantly affect the natural circulation response of PHTS whether to include the Z-Pipe heat losses or not, as shown in Figure 27. Nonetheless, it is clearly shown that the measurement of the thermal couple at IHX inlet is questionable. It matches neither the trend nor the magnitude with the simulation results for both cases with or without Z-Pipe heat losses. The measurement data are much higher at the beginning of the transient, while much lower during the later part of the transient.

Figure 28 shows the IHX heat removal rate during the SHRT-17 test. The IHX heat removal rate is significantly higher than the core power for the most of the test. This is expected since, unlike the ABTR PLOF transient, significant amount of flow rate were maintained for the intermediate heat transport system (IHTS) during SHRT-17 test. At the end of the 900-second test, the IHTS flow is still above 6% of the normal flow rate. The inner core and outer core flow rates are shown in Figure 29. It is clearly shown the flow reversal occurs for the average outer core channel between 60s and 130s. This is possible because the temperature in the outer core may be significantly lower than the inner core during certain period in the transient. Under natural circulation conditions, the differences in gravity head caused the flow reversal in the outer core and the pipes connected to the low-pressure inlet plenum. It can be confirmed that major flow responses in the primary coolant loop during the PLOF transient can be captured by the SFR Module simulation. A refinement of the EBR-II SHRT-17 model would include all leakages in the primary loop and a more detailed core for further EBR-II benchmark study.

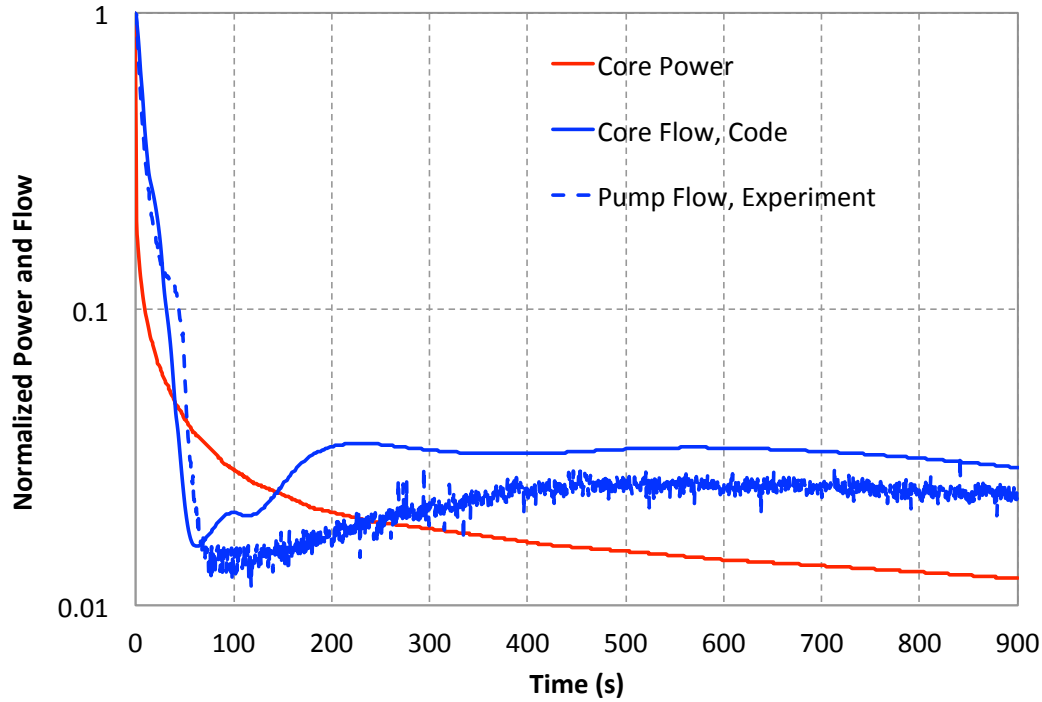

Figure 23: Comparison of core flow rate during the SHRT-17 test

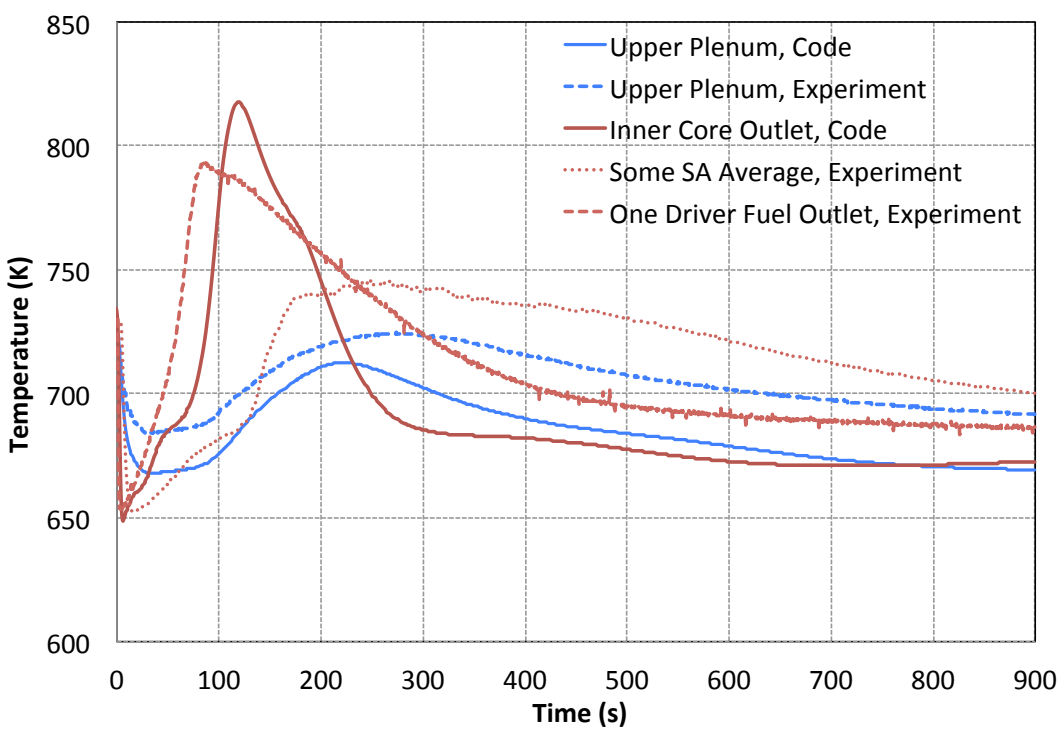

Figure 24: Comparison of core outlet temperatures during the SHRT-17 test

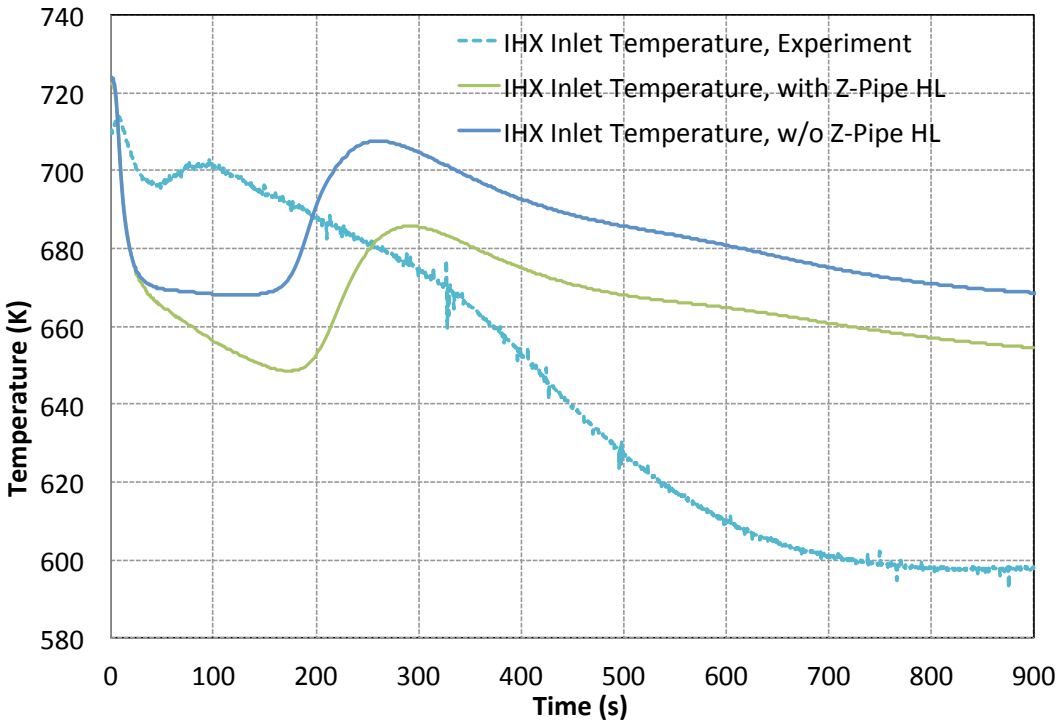

Figure 25: Comparison of IHX Inlet temperature during the transient

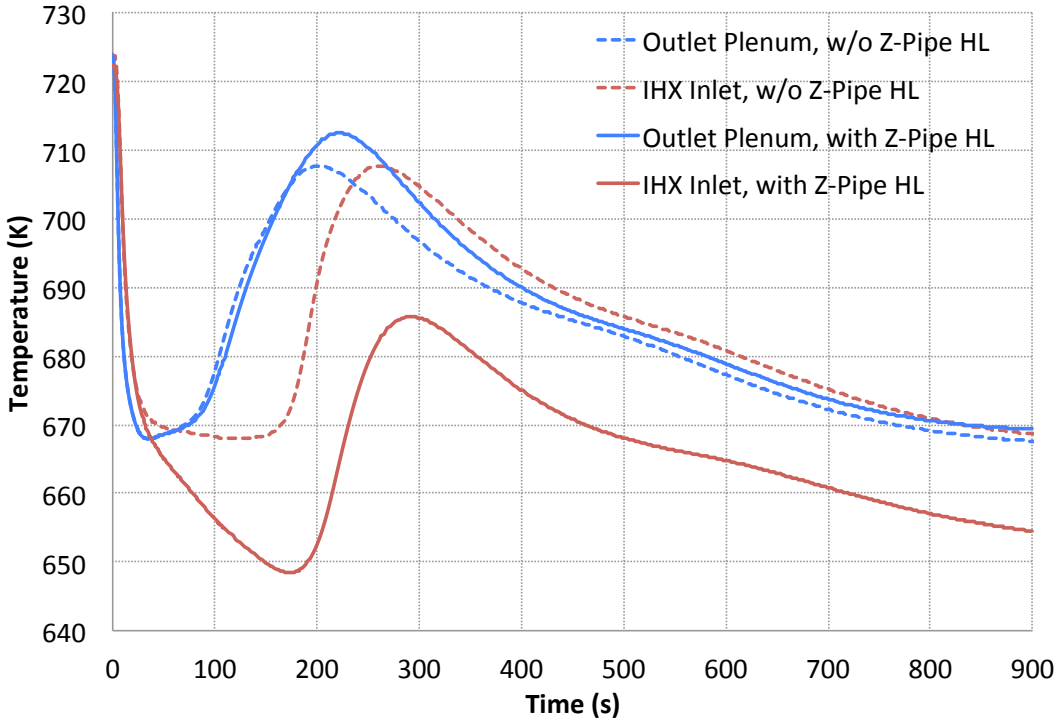

Figure 26: IHX inlet and outlet temperature responses, the effect of Z-Pipe heat loss

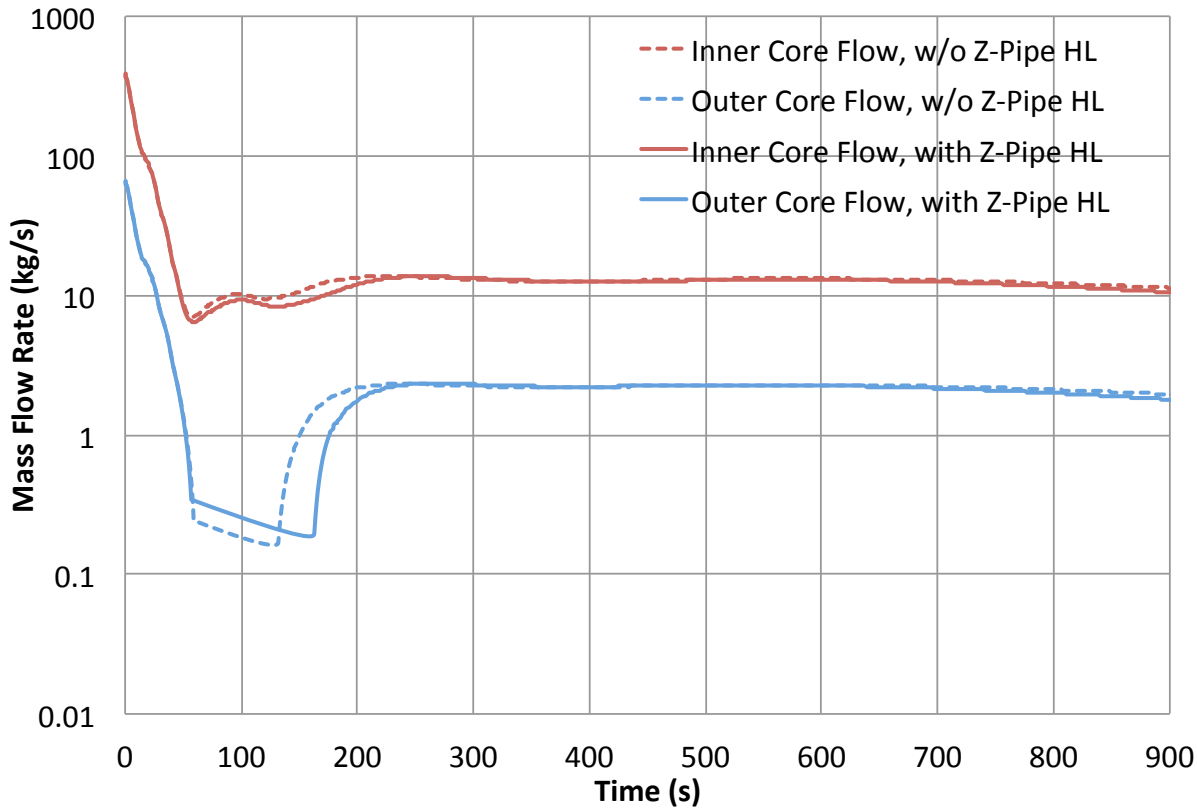

Figure 27: Core flow rate responses during SHRT-17 test, the effect of Z-Pipe heat loss

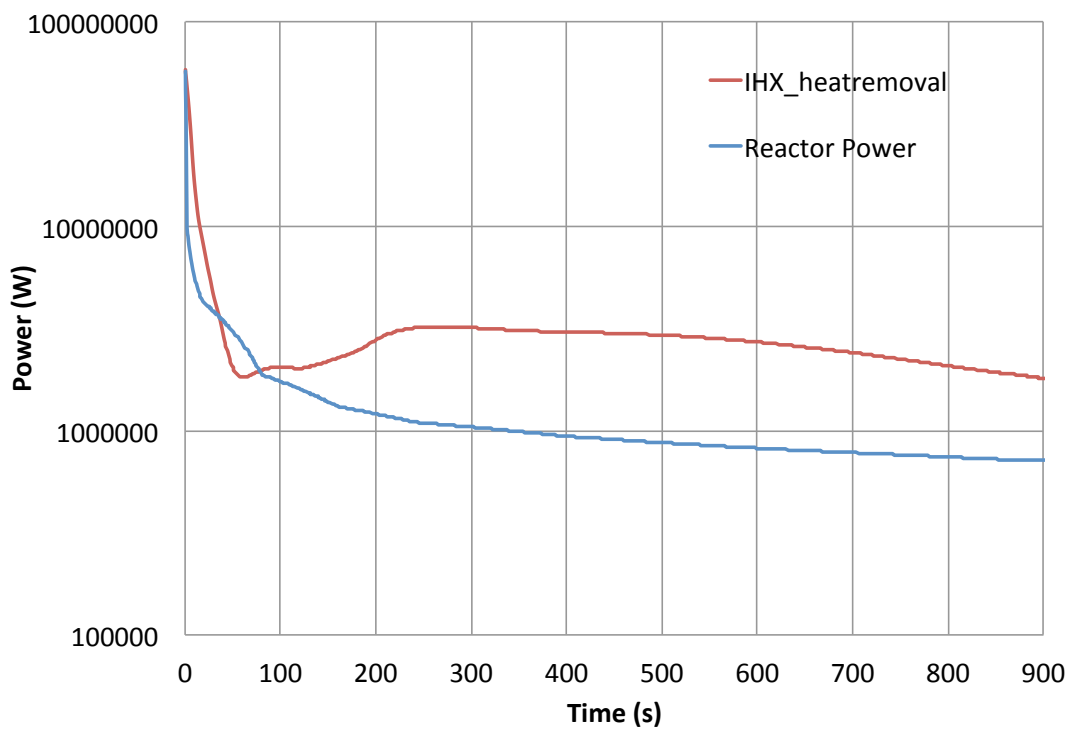

Figure 28: IHX heat removal rate response during the SHRT-17 test

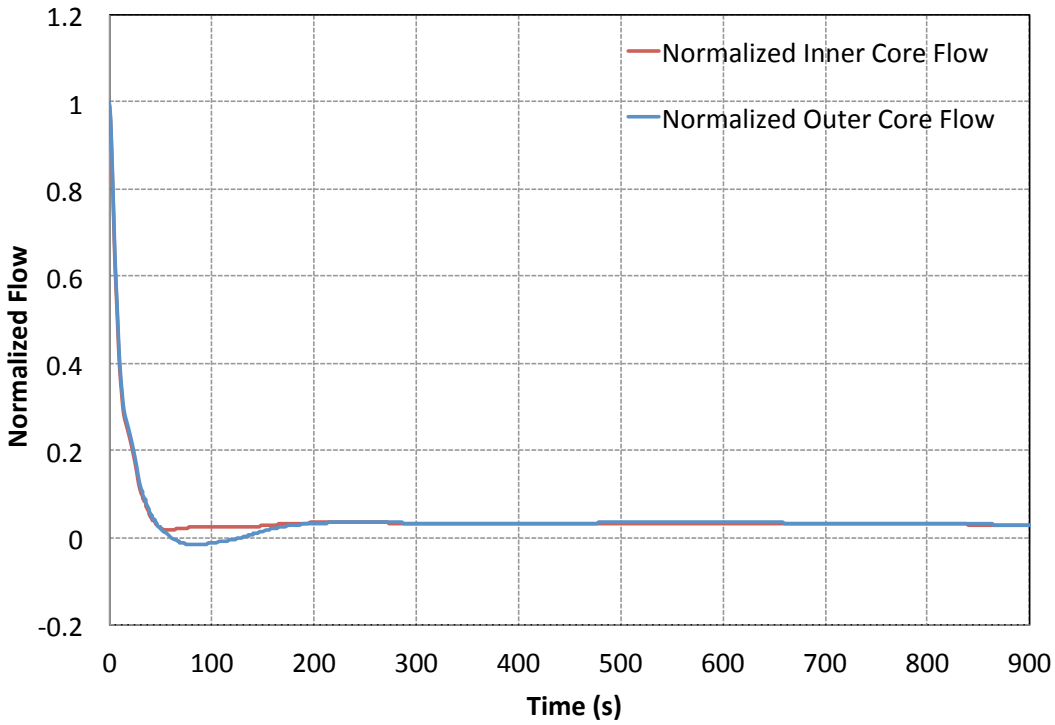

Figure 29: Inner and outer core flow responses during the SHRT-17 test

6 Summary

A SFR System Analysis Module is currently under rapid development. Although it is a relatively new effort, significant accomplishments have been achieved. In FY14, the 1-D FEM flow model using the pressure-based based formulation with numerical stabilization schemes has been improved for use in the incompressible sodium flows. It is confirmed that the developed FEM flow model can be strictly verified, and that it performs very well for a wide range of flow problems, including density wave propagation where numerical instability and numerical diffusion can be eliminated by its second-order numerical accuracy in both space and time; steep gradient problems where steep gradient can be handled and only slightly smoothed; discharging between tanks where flow reversal and a wide range of flow conditions (convection dominant or not) are modeled; and the flow and heat transfer in a heat exchanger where the conjugate heat transfer problem is accurately solved in a fully-coupled fashion.

A set of general and SFR-specific physics models and component has also been developed based on the pressure-based flow model. The simulation of the ABTR PLOF transient and the EBR-II SHRT-17 test has successfully demonstrated the SFR system simulation capabilities using the new set of Components, while also demonstrating its superior performance compared to the original density-based flow solver. The major physics phenomena in the primary coolant loop during the protected-loss-of-flow transients can be well captured during SFR System Analysis Module simulations. In the ABTR PLOF simulations, almost identical flow rates were predicted for both the pump coastdown and the natural circulation phases between the pressure-based and the density-based flow models. However, the computing time for the 1000 second transient is significantly reduced from ~2 hours to ~8 minutes with the pressure-based flow model. The transient response of the core flow in the simulation is also similar to that of the EBR-II SHRT-17 test, although the magnitudes are slightly different. Further investigations will be needed to resolve or better understand the causes of the differences between the simulation and experiment results.

Continued developments will be focused on component designs and physics integration for SFR analysis, demonstration of code capabilities through simulations of SFR design base accidents or design extension conditions, and code verification and validation. Additionally, the integration with other high-fidelity advanced simulation tools developed under the NEAMS Program, such as Nek-5000, will be investigated to pursue a multi-scale multi-physics simulation using the integrated NEAMS RPL tools.

REFERENCES

[1] RELAP5-3D Code Manual Volume 1: Code Structure, System Models and Solution Methods, INEEL-EXT-98-00834, Rev. 4, June 2012, http://www.inl.gov/relap5.

[2] M. Robert, M. Farvacque, M. Parent, and B. Faydide, "CATHARE 2 V2.5: A Fully Validated CATHARE Version for Various Applications," *Proc. 10th Int. Topl. Mtg. Nuclear Reactor Thermal Hydraulics* (NURETH 10), Seoul, Republic of Korea, October 5–9, 2003.

[3] T. H. Fanning, ed., The SAS4A/SASSYS-1 Safety Analysis Code System, Argonne National Laboratory, ANL/NE-12/4, January 31, 2012.

[4] D. Anders, R. Berry, D. Gaston, et al., "Demonstration of a Steady State Single Phase PWR Simulation with RELAP-7", INL/EXT-12-25924, Idaho National Laboratory, May 2012.

[5] D. Gaston, C. Newman, G. Hansen, and D. Lebrun-Grandi´e, "MOOSE: A parallel computational framework for coupled systems of nonlinear equations," *Nuclear Engineering and Design*, vol. 239, pp. 1768–1778 (2009).

[6] B. S. Kirk, J. W. Peterson, R. H. Stogner, and G. F. Carey, "libMesh: A C++ Library for Parallel Adaptive Mesh Refinement/Coarsening Simulations," *Engineering with Computers*, 22(3-4): 237-254 (2006).

[7] S. Balay, J. Brown, K. Buschelman, V. Eijkhout, W. D. Gropp, D. Kaushik, M. G. Knepley, L. C. McInnes, B. F. Smith, and H. Zhang, "PETSc Users Manual, ANL-95/11 – Revision 3.4," Argonne National Laboratory (2013).

[8] Y. I. Chang, P. J. Finck, C. Grandy, et al., "Advanced Burner Test Reactor Preconceptual Design Report," ANL-ABR-1 (ANL-AFCI-173), September 2006.

[9] T.E. Tezduyar, "Stabilized Finite Element Formulations for Incompressible Flow Computations," *Advances in Applied Mechanics*, Vol. 28, 1-44 (1992)

[10] R. Hu, J. W. Thomas, and T. H. Fanning, "Strategy for Multi-Scale Single-Phase Flow Coupling," ANL/NE-13/4, Argonne National Laboratory, March 2013.

[11] CD-adapco, "STAR-CCM+ 7.06 Manual," N.Y. (2012).

[12] R. Hu, J. W. Thomas, E. Munkhzul et al., "Development of SFR Primary System Simulation Capability for Advanced System Codes," ANL/NE-13/11, Argonne National Laboratory, September 2013.

[13] R. Hu, J. W. Thomas, E. Munkhzul, T. H. Fanning, "Coupled System and CFD Code Simulation of Thermal Stratification in SFR Protected Loss-Of-Flow Transients," *Proceedings of ICAPP 2014*, Charlotte, USA, April 6-9, 2014.

[14] A.N. Brooks, T.J.R.Hughes, "Streamline upwind/Petrov-Galerkin formulations for convection dominated flows with particular emphasis on the incompressible Navier-Stokes equations," *Comp. Methods Appl. Mech. Engrg.* , 32, 199 – 259 (1982).

[15] T.E. Tezduyar, "Stabilized Finite Element Formulations for Incompressible Flow Computations," *Advances in Applied Mechanics*, Vol. 28, 1-44 (1992)

[16] D. A. Knoll and D. E. Keyes, "Jacobian-free Newton-Krylov Methods: a Survey of Approaches and Applications," *Journal of Computational Physics*, Vol. 193, pp.357–397 (2004).

[17] T.S. Sumner, T.Y.C. Wei, A. Moisseytsev, A. Mohamed, L.L. Briggs, unpublished information, Argonne National Laboratory (2012).

[18] T.S. Sumner, personal communication (2014).

Nuclear Engineering Division
Argonne National Laboratory
9700 South Cass Avenue
Argonne, IL 60439

www.anl.gov

Argonne National Laboratory is a U.S. Department of Energy laboratory managed by UChicago Argonne, LLC